

Original Article

Cite this article: Yang J, Liu W, Han Z, Zeng Z, Wan L, and Mohammed AS (2021) Petrogenesis of Silurian ultramafic–mafic plutons in southern Jiangxi: implications for the Wuyi–Yunkai orogen, South China. *Geological Magazine* 158: 1237–1252. <https://doi.org/10.1017/S0016756820001272>

Received: 18 May 2020

Revised: 16 October 2020

Accepted: 22 October 2020

First published online: 4 December 2020

Keywords:

Wuyi–Yunkai orogen; ultramafic–mafic plutons; high MgO; Silurian; South China

Authors for correspondence:

Wei Liu, Email: weiliu_2019@tju.edu.cn;

Zuozhen Han, Email: hazz@163.com

Petrogenesis of Silurian ultramafic–mafic plutons in southern Jiangxi: implications for the Wuyi–Yunkai orogen, South China

Jie Yang¹, Wei Liu² , Zuozhen Han^{1,3}, Zuoxun Zeng⁴, Le Wan⁴ and Adil S. Mohammed⁴

¹Shandong Provincial Key Laboratory of Depositional Mineralization and Sedimentary Minerals, College of Earth Science and Engineering, Shandong University of Science and Technology, Qingdao 266590, PR China; ²Institute of Surface-Earth System Science, Tianjin University, Tianjin 300072, PR China; ³Laboratory for Marine Mineral Resources, Qingdao National Laboratory for Marine Science and Technology, Qingdao 266237, PR China and ⁴School of Earth Sciences, China University of Geosciences, Wuhan 430074, PR China

Abstract

The South China Block is one of the largest continental blocks located on the East Asian continent. The early Palaeozoic Wuyi–Yunkai orogen of the South China Block (known as the Caledonian orogen in Europe) is a major orogenic belt in East Asia and represents the first episode of extensive crustal reworking since Neoproterozoic time. Although this orogen is key to deciphering the formation and evolution of the South China Block, details about the orogen remain poorly defined. The Songshutang and Wushitou ultramafic–mafic units in southern Jiangxi Province, South China, have ²⁰⁶Pb–²³⁸U ages of *c.* 437 Ma, suggesting a Silurian formation age. All the Songshutang and Wushitou ultramafic–mafic rocks show relatively flat chondrite-normalized rare earth element patterns, depletions in Nb, Ta, Zr, Hf and Ti, and low $\epsilon_{\text{Nd}}(t)$ values from -9.12 to -5.49 with negative zircon $\epsilon_{\text{Hf}}(t)$ values from -10.84 to -2.58 , resembling a typical arc magma affinity. Geochemical and isotopic data indicate that the newly identified ultramafic–mafic rocks, along with the reported Silurian mafic rocks in South China, possibly originated from the similar partial melting of an ancient subducted slab, fluid/sediment and metasomatized lithospheric mantle with varying degrees of fractional crystallization. In conjunction with other records of magmatism and metamorphism in South China, a late-orogenic extensional event led to the melting of the sub-continental lithospheric mantle in Silurian time and generated ultramafic–mafic rocks with a limited distribution along the Wuyi–Yunkai orogen and widespread late-orogenic granitic plutons in the South China Block.

1. Introduction

China was aggregated from three major Precambrian blocks during the Phanerozoic Eon: the South China, North China and Tarim blocks (Zhao & Cawood, 2012). The South China Block (SCB) is a major continental block and occupies the bulk of southern China. It is traditionally considered to be separated from the North China Block by the Qinling–Dabie–Sulu orogen (Wang *et al.* 2013a) and evolved over a long-lived accretion–collision history from Proterozoic to Mesozoic times (Lin *et al.* 2018; Liu *et al.* 2018). The early Palaeozoic NE–SW-trending Wuyi–Yunkai orogen is a major orogenic belt in South China (Li *et al.* 2010). This orogen possibly stretches ~2000 km to the NE Korean Peninsula and SW Indochina Block and covers the southeastern half of the SCB (Fig. 1). This orogenic event, also regarded as the ‘Caledonian Orogeny’ and/or ‘Kwangian Orogeny’ in Chinese literature, is correlated with the Caledonian orogen in Europe (e.g. Huang, 1980; Ren, 1991; Wang *et al.* 2007; Zeng *et al.* 2008; Li *et al.* 2010; Zhang, Q. *et al.* 2015). The Wuyi–Yunkai orogen is marked by a regional angular unconformity between Middle Devonian strata and pre-Devonian strata in the eastern SCB (Cathaysia Block) (e.g. Li *et al.* 2010; Zhang *et al.* 2017), the absence of upper Silurian sediments, intensive deformation, extensive folding of pre-Devonian rocks and widespread early Palaeozoic granitoid intrusions (e.g. Charvet *et al.* 2010; Li *et al.* 2017). The core of this orogen is defined by a zone of NE-trending regional upper-greenschist to granulite-facies metamorphism (e.g. Wang *et al.* 2013b; Yu *et al.* 2019).

Early Palaeozoic granitic rocks in the SCB are the main product of this orogenic event and are dominated by peraluminous gneissoids and massive granites. These granitic rocks crystallized between 400 and 470 Ma with a peak age of ~436 Ma and have a geochemical affinity to S- and I-type granites (Wang *et al.* 2013b and reference therein). Numerous studies have been carried out on the origin and tectonic evolution of the Wuyi–Yunkai orogen; however, there are still controversies about whether it was an intracontinental orogen (e.g. Faure *et al.* 2009; Charvet *et al.* 2010; Feng *et al.* 2014; Peng *et al.* 2015; Zhang, Q. *et al.* 2015; Wang *et al.* 2017; Ou *et al.*

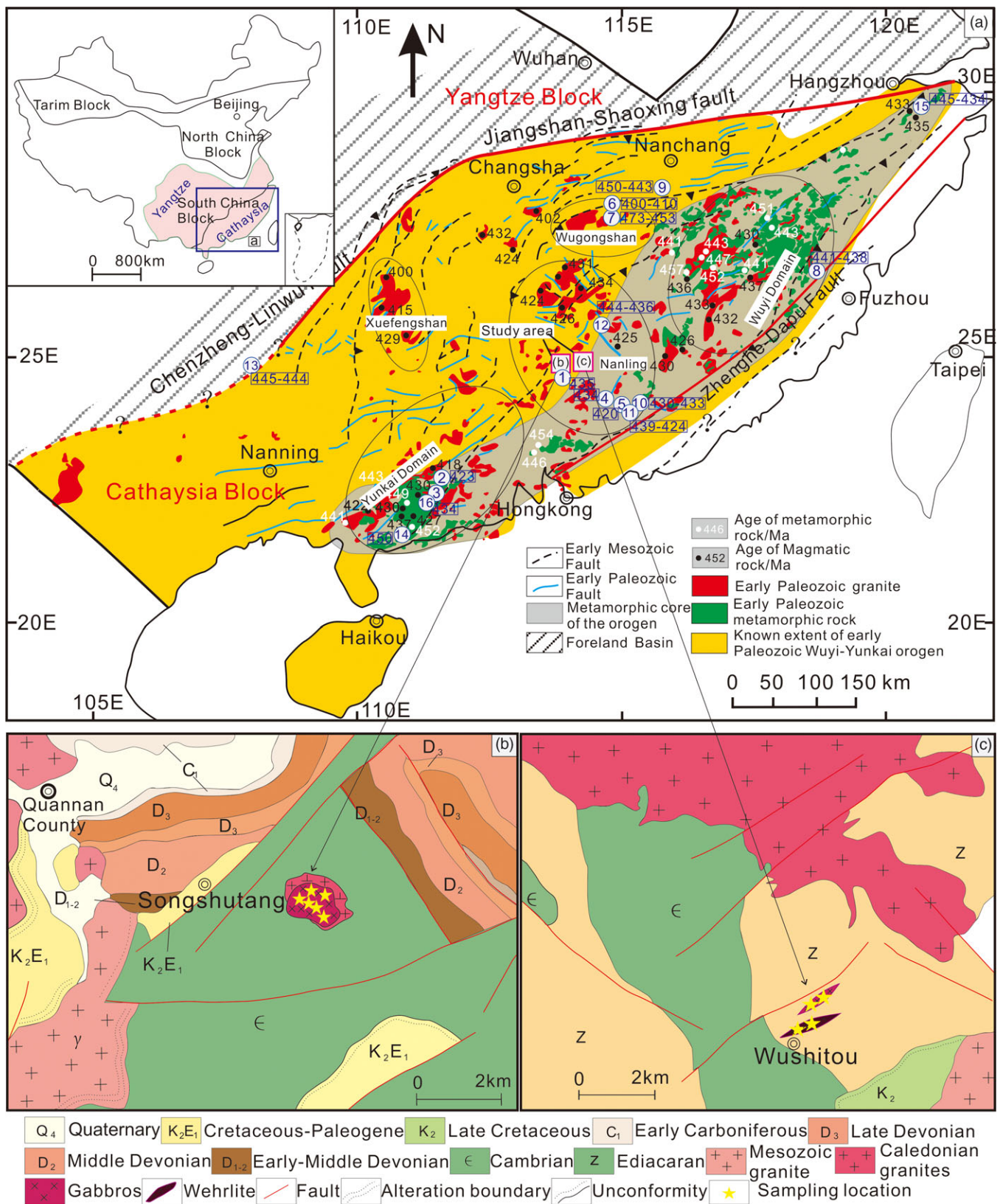


Fig. 1. (Colour online) (a) A simplified regional geological map of eastern South China showing the distributions of the early Palaeozoic Wuyi-Yunkai orogen (modified from Yao et al. 2012 and Huang & Wang, 2019). Sources for existing Ordovician-Silurian ultramafic-mafic rocks are from: 1 – Silurian Chayuanshan volcanic succession, Guangdong, Yao et al. (2012); 2 – Silurian Longhugang gabbroic pluton, Northern Yunkai, Wang et al. (2013b); 3 – Silurian Zhouya-Shiban gabbroic pluton, Northern Yunkai, Wang et al. (2013b); 4 – Silurian Xinchuan gabbroic pluton, Southern Nanling, Wang et al. (2013b); 5 – Silurian Xinsi gabbroic pluton, Southern Nanling, Wang et al. (2013b); 6 – Taoyuan hornblende gabbro, Jiangxi, Zhong et al. (2013); 7 – Ordovician Eastern Wugongshan appinites, Jiangxi, Zhong et al. (2014); 8 – Silurian Dakang gabbroic pluton, Fujian, Zhang, Q. et al. (2015); 9 – Ordovician Songxi mafic intrusions, Jiangxi, Zhang, C. L. et al. (2016); 10 – Silurian Yonghe hornblende gabbro, Guangdong, Xu et al. (2017); 11 – Silurian Longchuan, Longmu and Huwei gabbro-diorites, Guangdong, Jia et al. (2017); 12 – Silurian Tangshan and Danqian diorites, Jiangxi, Jia et al. (2017); 13 – Silurian Danling lamprophyre, Guangxi, Jia et al. (2017); 14 – Ordovician Zhuya gabbro, Guangdong, Yu, P. et al. (2018); 15 – Silurian Chencai mafic rocks, Zhejiang, Li et al. (2017) and Zhao et al. (2019); 16 – Silurian Chidong gabbro, Northern Yunkai, Xu et al. (2019). (b) A simplified geological map of the Songshutang area. (c) A simplified geological map of the Wushitou area.

2018; Xie *et al.* 2020) or an ocean subduction–collisional orogen (e.g. He *et al.* 2014; Peng *et al.* 2016; Chen *et al.* 2015; Zhang, C. L. *et al.* 2016). According to these tectonic models, this orogeny is regarded as a consequence of the far-field stress of the collision between the SCB and NE Gondwana (e.g. Li *et al.* 2010; Yao & Li, 2019; Wang *et al.* 2020) or of arc or continental collisions following the closure of the residual Huanan Ocean between the Yangtze and Cathaysia blocks (Liu *et al.* 2018).

Unlike the extensive occurrence of early Palaeozoic granitic plutons and metamorphic events in the Wuyi–Yunkai orogen, details of synchronous ultramafic–mafic rocks, which are important for unravelling the origin of the orogen and understanding the evolution of the crust and mantle beneath it, remain unclear (Fig. 1a and references therein). Peng *et al.* (2006) proposed that the ultramafic–mafic plutons were part of the ophiolite complex caused by the closure of the ‘Palaeo South China Ocean’ in early Palaeozoic time. In contrast, Zhang, C. L. *et al.* (2015) demonstrated that the early Palaeozoic mafic rocks were formed under a continental–continental collision orogeny. The model of partial melting of ancient lithospheric mantle or mantle wedge as a consequence of lithospheric delamination within an intracontinental regime during early Palaeozoic time has been widely accepted by most scholars (e.g. Yao *et al.* 2012; Wang *et al.* 2013b; Zhong *et al.* 2014; Zhang, Q. *et al.* 2015; Zhang, C. L. *et al.* 2016; Jia *et al.* 2017; Liu *et al.* 2020). More data and evidence are required to improve our understanding of the nature and evolution of the early Palaeozoic ultramafic–mafic rocks and orogenic events in the SCB. Wehrlite and high-MgO gabbroic rocks represent the least evolved primary melt, which records pivotal information about the mantle thermochemical state. Our recent investigations identified several Silurian wehrlite and high-MgO mafic plutons in southern Jiangxi Province, South China (Fig. 1b, c). In this study, we perform comprehensive petrological, zircon U–Pb age and whole-rock geochemical and Nd isotope analyses of these rocks. Based on the analysed data, we deduce the petrogenesis of the ultramafic–mafic rocks in this region and provide pivotal information about the tectonic setting of the Wuyi–Yunkai orogen in the SCB.

2. Geological background

The SCB is thought to have formed from the amalgamation of the Yangtze Block and Cathaysia Block during early Neoproterozoic time along the Jiangnan orogen (e.g. Li *et al.* 2002; Li & Li, 2007; Zhao & Cawood, 2012; Cawood *et al.* 2013; Hu *et al.* 2017). The Yangtze Block is composed of Archaean–Palaeoproterozoic crystalline basement whereas the Cathaysia Block consists of Palaeo–Neoproterozoic lithologies with no exposed Archaean basement (e.g. Zhao & Cawood, 2012; Cawood *et al.* 2013; Hu *et al.* 2014; Wang *et al.* 2013b). Neoproterozoic – early Palaeozoic low-grade/non-metamorphic deposits (Charvet *et al.* 2010; Yao *et al.* 2012; Xia *et al.* 2014) and Palaeoproterozoic – early Neoproterozoic high-grade metamorphic complexes (Zhao & Cawood, 1999; Cawood *et al.* 2013) are preserved in both the Yangtze and the Cathaysia blocks.

Multiple tectonic events have reshaped the SCB during Phanerozoic time (Zhao *et al.* 2019), such as the early Palaeozoic Wuyi–Yunkai orogeny (Kwangsonian tectonic event), the Triassic Indosinian event and the Jurassic–Cretaceous Yanshanian event (e.g. Ren, 1991; Zhao & Cawood, 1999; Faure *et al.* 2009; Charvet *et al.* 2010; Cawood *et al.* 2013; Wang *et al.* 2013b; Yang *et al.* 2013; Xia *et al.* 2014; Zhang *et al.* 2019).

The early Palaeozoic Wuyi–Yunkai orogeny is considered to be the first critical period during which extensive magmatic and metamorphic activities developed (Huang & Wang, 2019) and many areas of the present-day crystalline basement in the SCB were reworked (Zhao *et al.* 2019). As a result of this orogeny, massive quantities of sediments were shed in the evolving Nanhua basin, and a large fold-and-thrust system developed (e.g. Li *et al.* 2013; Yao & Li, 2016). Most upper Neoproterozoic – Ordovician strata in the SCB have experienced upper-greenschist–granulite-facies metamorphism and are unconformable with the overlying Middle Devonian – Lower Triassic lower-greenschist-facies metamorphic rocks (e.g. Wang & Li, 2003; Hu *et al.* 2018). The unconformity between the upper and lower Palaeozoic packages is distributed widely in the eastern Yangtze Block and Cathaysia Block (Wang *et al.* 2013b and references therein).

A large amount of precise geochronological data from associated magmatic and metamorphic rocks indicate that this early orogeny occurred between > 460 Ma (Middle Ordovician) and c. 415 Ma (around the Silurian–Devonian boundary) (e.g. Carter *et al.* 2001; Kim *et al.* 2006; Wang *et al.* 2007, 2013a; Li *et al.* 2010; Xia *et al.* 2014; Yu *et al.* 2019), and this event was named after the widespread Ordovician–Devonian peraluminous gneissic and post-kinematic granites along the NE–SW-trending Wuyi–Yunkai Mountains (e.g. Ren, 1991; Charvet *et al.* 2010; Li *et al.* 2010; Wang *et al.* 2013b; Zhang, J. *et al.* 2016; Fig. 1a). These granitic plutons, which were considered representative of the magmatic response to this orogen (Xu *et al.* 2016), generally intruded into the Neoproterozoic–Cambrian metamorphic basement rocks and can be divided into two stages based on their geographic distributions and petrographic characteristics (Huang & Wang, 2019). The 450–430 Ma granitic rocks are widely distributed in the Wugongshan, Wuyi and Yunkai areas and are generally characterized by a gneissic texture with strong peraluminous compositions (e.g. Zhong *et al.* 2013; Xu & Xu, 2017; Qiu *et al.* 2018). Granitic rocks with ages of 440–400 Ma are mainly exposed in the Xuefengshan and Nanling areas and are usually massive with geochemical compositions approaching metaluminous I-type granites (e.g. Shu *et al.* 2015; Song *et al.* 2015).

A zone of NE-trending regional upper-greenschist to granulite-facies metamorphism developed along the Wuyi–Yunkai region (Li *et al.* 2010; Yu *et al.* 2019). Early Palaeozoic granulites with a typical collision-related clockwise metamorphic *P–T* path are only distributed in the southeastern Cathaysia Block (Yu *et al.* 2019). Early Palaeozoic Cathaysia sequences are extensively overprinted by strong folding, thrusting and strike-slip shearing, whereas no coeval significant deformation has been found in the Yangtze Block (e.g. Charvet, 2013; Shu *et al.* 2015).

Recently, Ordovician and Silurian mafic plutons and volcanic rocks were reported in northern and western Guangdong (Yao *et al.* 2012; Wang *et al.* 2013b; Jia *et al.* 2017; Yu, P. *et al.* 2018; Xu *et al.* 2019), northern and southern Jiangxi (Zhong *et al.* 2014; Zhang, C. L. *et al.* 2016; Jia *et al.* 2017), northern Guangxi (Jia *et al.* 2017), central Fujian (Zhang, Q. *et al.* 2015) and central Zhejiang (Li *et al.* 2017; Zhao *et al.* 2019) (Fig. 1a). The early Palaeozoic Wuyi–Yunkai orogeny was further divided into an Ordovician primary compression stage and a Silurian collapse stage based on these new findings (Yao & Li, 2019). In our recent regional geological survey, a series of ultramafic–mafic plutons were identified in the Songshutang and Wushitou areas of southern Jiangxi Province in the Cathaysia Block.



Fig. 2. (Colour online) Field photographs of the Songshutang and Wushitou ultramafic-mafic rocks in South China Block: (a–c) gabbro and leucogabbro of the Songshutang intrusions; (d–f) olivine-gabbro of the Songshutang intrusions; (g–i) Wushitou wehrlite. Length of hammer used for scale is ~30 cm; diameter of coin used for scale is ~1.7 cm.

3. Sampling and petrology

3.a. Geology of the Songshutang and Wushitou ultramafic-mafic rocks

The Songshutang mafic pluton is located in the Dingnan area, southern Jiangxi Province, South China (Fig. 1b; 24° 43' N, 114° 35' E). The pluton intruded into granodiorite and Cambrian Shuishi Formation siltstones in a NW–SE direction with an overall plane circular shape covering ~0.5 km². The mafic intrusions consist mainly of dark green olivine-gabbro, gabbro and leucogabbro gradually changing from the centre to the margin (Fig. 2a–f). Leucogabbro samples G07-2, G07-2-1 and G07-3, gabbro samples G07-5 and G07-5-1 and olivine-gabbro samples G07-4 and G07-4-1 were collected from the margin to the centre of the Songshutang intrusion.

The Wushitou ultramafic-mafic plutons are located in Dingnan County, southern Jiangxi Province (Fig. 1c; 24° 41' N, 115° 06' E). The lenticular-shaped ultramafic-mafic rocks, consisting of dark green wehrlite (Fig. 2g–i) and gabbro, intruded into the Ediacaran migmatites and/or metamorphic rocks, which stretch NE–SW up to hundreds of metres long (Fig. 2g). The two intrusions are separate from each other (Fig. 1). Two samples (G10-1 and G10-1-1) were collected from the mafic (gabbro) pluton,

and two samples (G10-2 and G10-2-1) were collected from the ultramafic (wehrlite) pluton.

3.b. Petrology of the Songshutang and Wushitou intrusions

The olivine-gabbro samples (G07-4 and G07-4-1) from the Wushitou and Songshutang intrusions are massive with euhedral clinopyroxene (~35%), plagioclase (~50%), amphibole (~5%) and minor olivine (less than 5%) and Fe–Ti oxides (5–10%) (Fig. 3a, b). The gabbro samples in the Wushitou (G07-5 and G07-5-1) and Songshutang (G10-1 and G10-1-1) intrusions are massive with euhedral clinopyroxene (~30%), amphibole (~5%), plagioclase (~60%) and Fe–Ti oxides (~5%) (Fig. 3a, b). The leucogabbro samples (G07-2, G07-2-1 and G07-3) in the Wushitou intrusion have euhedral clinopyroxene (~25%), plagioclase (~70%) and minor Fe–Ti oxides (less than 5%). The grains of clinopyroxene, plagioclase and olivine in all samples are between 0.1 mm and 0.5 mm in size and are interspersed with each other (Fig. 3a, b). A small amount of plagioclase was altered to sericite, and clinopyroxene was altered to sericite. This is consistent with the slightly higher loss on ignition (LOI) percentages (Fig. 3a, b; online Supplementary Material Table S4). The wehrlite rocks are massive and coarse grained (0.1–1 mm) with a slight cumulate

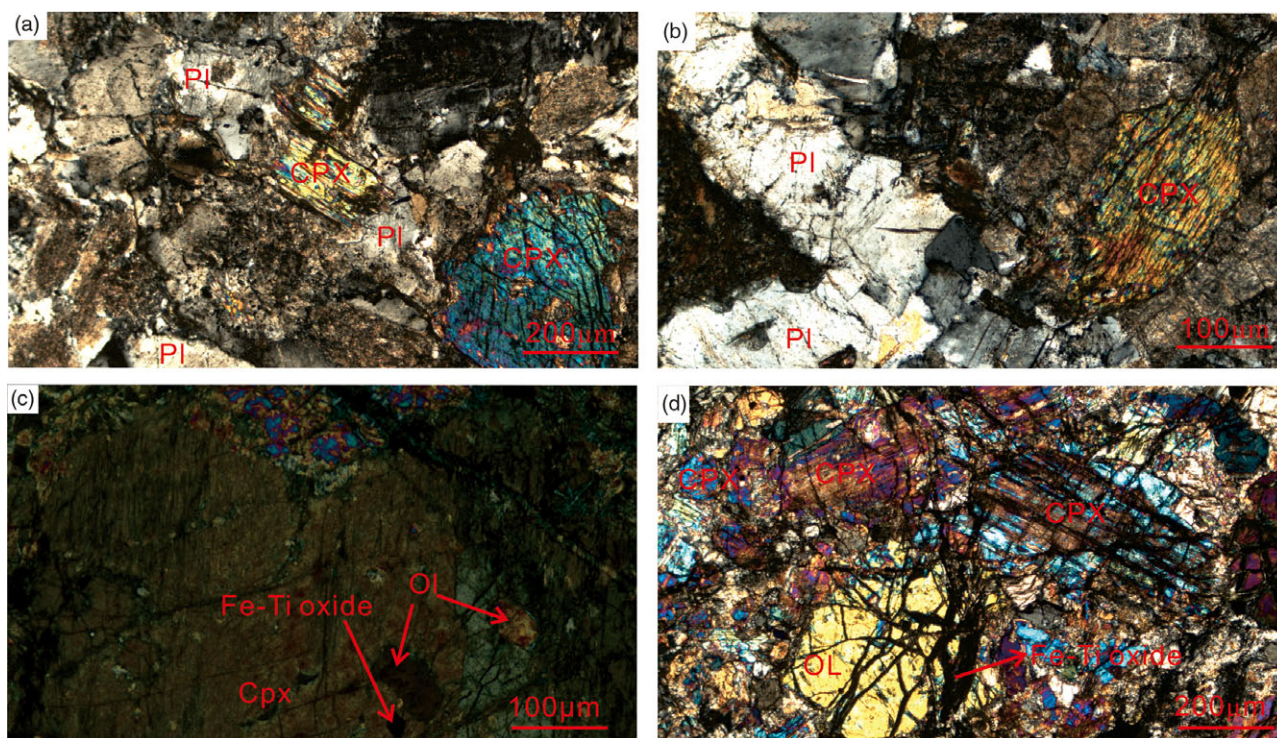


Fig. 3. (Colour online) Photomicrographs of the Songshutang and Wushitou ultramafic–mafic rocks in South China Block: (a) gabbro of the Songshutang intrusions; (b) leucogabbro of Songshutang intrusions; (c, d) Wushitou wehrlite. Ol – olivine; Cpx – clinopyroxene; Pl – plagioclase.

structure and consist of olivine (~50%), clinopyroxene (~35%) and Fe–Ti oxides (~15%) (Fig. 3c, d). Olivine (~0.1 mm) enclosed in large clinopyroxene (0.5–1 mm), forming a poikilitic texture, is also preserved in the wehrlite of the Wushitou intrusions (Fig. 3c). Portions of olivine and clinopyroxene in the wehrlite were altered to serpentine and sericite and chlorite, respectively, consistent with the high LOI percentages (online Supplementary Material Table S4).

4. Analytical methods

Eleven fresh ultramafic–mafic samples were collected from the Songshutang and Wushitou areas. Whole-rock major- and trace-element compositions and Sr–Nd isotopic analyses, and zircon U–Pb age dating, trace-element and Hf isotope analyses were conducted on these samples.

Zircons from gabbro samples G07-5 and G10-1 and leucogabbro samples G07-2 and G07-3 were selected for *in situ* U–Pb isotope analysis. Conventional heavy liquid and magnetic techniques were used for zircon selection under a binocular microscope at the Langfang Integrity Geological Services Incorporation. The high-resolution cathodoluminescence (CL) images of zircons were carried out using a JXA-8100 electron microscope at the State Key Laboratory of Geological Processes and Mineral Resources, China University of Geosciences in Wuhan (SKLGPMP, CUG). Zircon U–Pb dating and trace-element composition analyses were performed synchronously at the LA-ICP-MS laboratory of GPMR using an Agilent 7700a inductively coupled plasma mass spectrometer (ICP-MS). Laser ablation experiments were conducted using the GeoLas 200M laser-ablation system (MicroLas, Göttingen, Germany). The beam diameter was 32 μm. Zircon 91500 was used as an external standard, ^{29}Si was used as an internal standard and NIST SRM610 was used as a reference material for calculating the element contents. The errors on single data points were quoted at

the 1σ level, and the uncertainties in ages were quoted at the 95% confidence level (2σ). Detailed analytical methods were similar to those described by Yang *et al.* (2019b) and Shan *et al.* (2004).

In situ zircon Hf isotope analysis was conducted at the GPMR using a Neptune Plus multi-collector ICP-MS (Thermo Fisher Scientific, Germany). Zircons 91500 and GJ-1 were measured for external calibration twice every five analyses of the zircon samples and yielded weighted mean $^{176}\text{Hf}/^{177}\text{Hf}$ values of 0.282303 ± 8 ($n = 15$, 1σ) and 0.282009 ± 6 ($n = 15$, 1σ), respectively. The detailed analytical procedure was described by Hu *et al.* (2008).

Whole-rock major-element concentrations were measured with an XRF-1800 sequential X-ray fluorescence (XRF) spectrometer at GPMR. The analytical precision (RSD) for major elements was better than 4%, and the accuracy (RE) was better than 3%. Trace and rare earth element (REE) analyses were determined by an Agilent 7500a ICP-MS at GPMR. The AGV-2, BHVO-2, BCR-2 and GSR-3 standards were used for calibration, and the analytical precision was better than 5%. Whole-rock Sr–Nd isotopic ratios were determined at GPMR using a Finnigan Triton thermal ionization mass spectrometer (TIMS). The NBS987 and La Jolla standards, which yielded weighted mean $^{87}\text{Sr}/^{86}\text{Sr}$ ratios of 0.710254 ± 0.000008 (2σ) and weighted mean $^{143}\text{Nd}/^{144}\text{Nd}$ ratios of 0.511847 ± 0.000003 (2σ), respectively, were used for calibration. Isotopic ratios of $^{87}\text{Sr}/^{86}\text{Sr} = 8.375209$ and $^{143}\text{Nd}/^{144}\text{Nd} = 0.721900$ were used for the mass fractionation corrections. Detailed analytical methods were described by Ma *et al.* (2012) and Yang *et al.* (2019a).

5. Results

5.a. Zircon U–Pb age and trace elements

LA-ICP-MS zircon U–Pb dating and trace-element results for three samples of the Songshutang gabbro and one sample of the

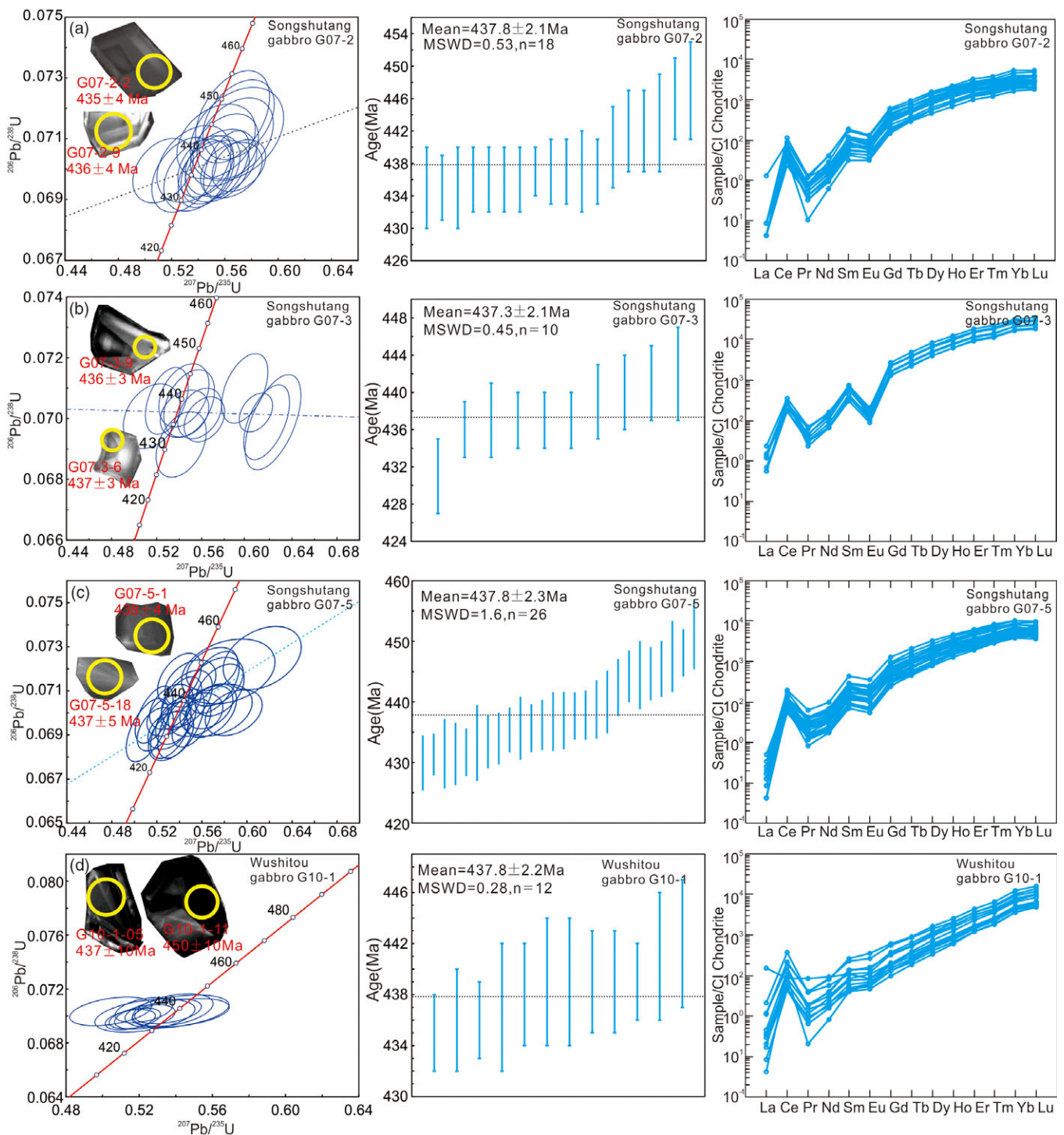


Fig. 4. (Colour online) Concordia zircon U–Pb age and chondrite-normalized zircon trace-element pattern diagrams for the Songshutang and Wushitou gabbros in the SCB. The yellow circles on the CL images represent the LA-ICP-MS age spots; ellipse dimensions are 1 σ ; spot diameter is 32 μ m.

Wushitou gabbro are listed in online Supplementary Material Tables S1 and S2. Most of the zircon crystals are colourless and transparent and display well-developed prismatic crystal morphology and CL images with wide oscillatory zoning with lengths between 50 and 100 μ m (Fig. 4). These characteristics are consistent with zircons from mafic rocks, which exhibit wider oscillatory zones than zircons from granite (Wu & Zheng, 2004). All analysis spots contain high Th/U ratios (> 1) and are characterized by typically steep

chondrite-normalized REE patterns ($Gd_N/Yb_N = 0.02\text{--}0.14$) with positive Ce (1.5–11) and negative Eu (0.04–0.40) anomalies (Fig. 4). These characteristics are consistent with a magmatic origin (Hoskin & Ireland, 2000; Hoskin & Schaltegger, 2003), and the zircon U–Pb age could represent the crystallization age of these mafic plutons.

Twenty analyses of 20 zircons were undertaken on Songshutang gabbro G07-2, and all ages display concordance greater than 90 %.

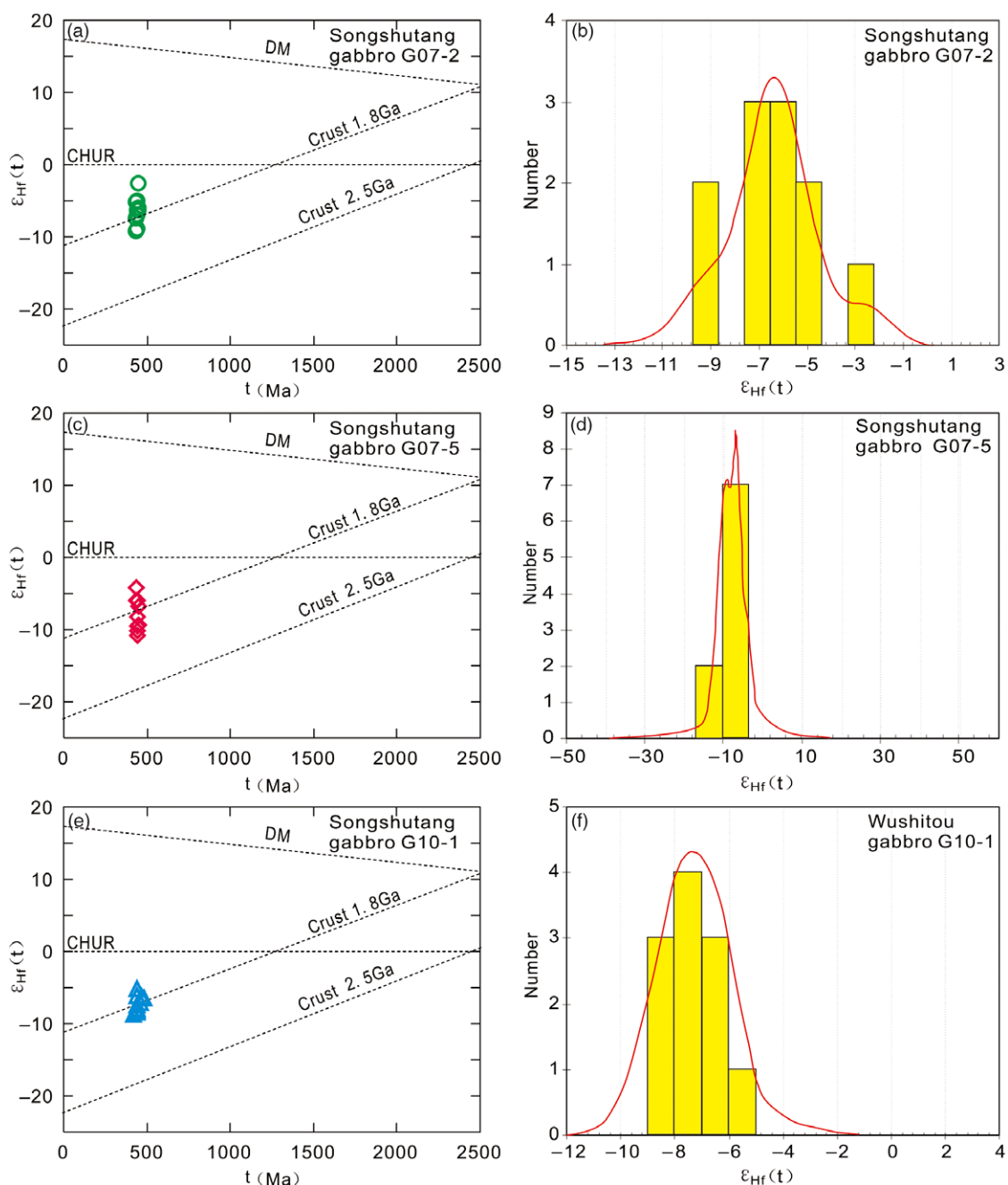


Fig. 5. (Colour online) (a, c, e) $\epsilon_{\text{Hf}}(t)$ value versus crystallization age diagrams, and (b, d, f) histograms of the zircon $\epsilon_{\text{Hf}}(t)$ for the Songshutang and Wushitou samples.

Eighteen of 20 analysis spots gave a weighted mean ^{206}Pb – ^{238}U age of 437.8 ± 2.1 Ma (MSWD = 0.53, ranging from 447 to 435 Ma). Spots G07-2-18 and 19 provided older ^{206}Pb – ^{238}U ages of 2505 and 2376 Ma, respectively, which are interpreted to be the ages of inherited zircons. Thirteen spots were analysed from Songshutang gabbro G07-3, and 11 analyses yielded concordant ages ranging from 442 to 431 Ma (except G07-3-8 = 1325 Ma). Ten analysis spots gave a weighted mean ^{206}Pb – ^{238}U age of 437.3 ± 2.1 Ma (MSWD = 0.45). Twenty-seven spots were selected for zircon U–Pb dating from Songshutang gabbro G07-5; 26 analysis spots yielded concordant ages ranging from 447 to 431 Ma and gave a weighted mean ^{206}Pb – ^{238}U age of 437.8 ± 2.3 Ma (MSWD = 1.6) (Fig. 4).

Twenty-one analysis spots on 21 zircon grains were selected from Wushitou gabbro G10-1 for zircon U–Pb dating, 20 of which yielded concordant ages. Twelve analysis spots gave a weighted mean ^{206}Pb – ^{238}U age of 437.8 ± 2.2 Ma (MSWD = 0.28, ranging from 442 to 435 Ma).

5.b. Zircon Hf isotopes

A total of 31 analysis spots distributed among the zircon grains from the Songshutang samples G07-2 and G07-5 and Wushitou sample G10-1 were selected for zircon Hf isotope analysis. The results are presented in online Supplementary Material Table S3 and Figure 5. Eleven analysis spots for sample G07-2 yielded

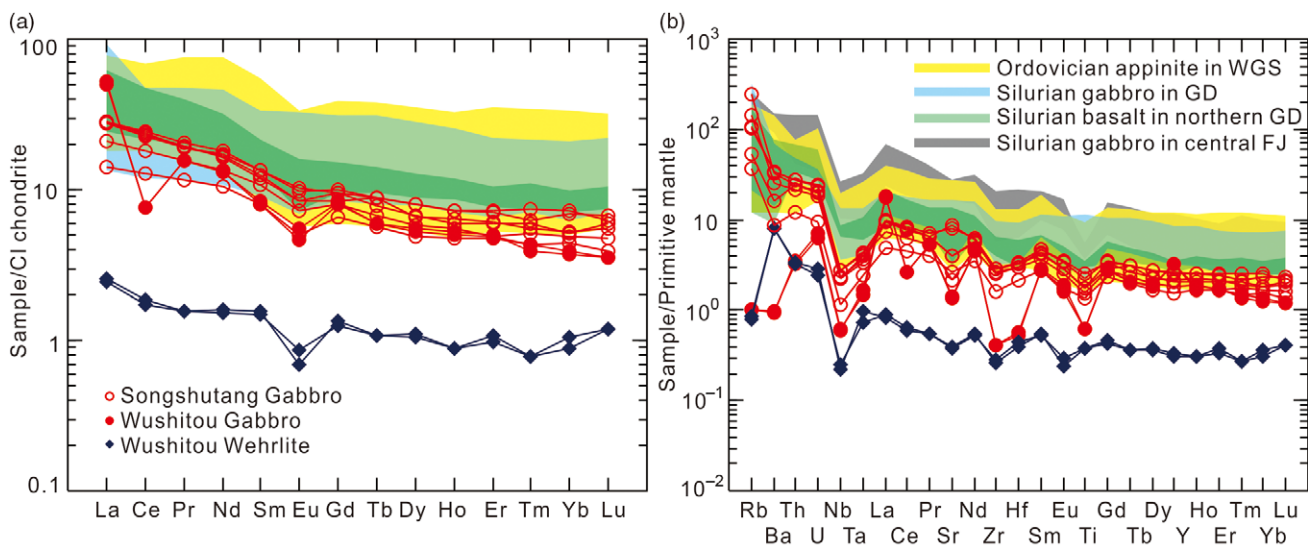


Fig. 6. (Colour online) (a) Chondrite-normalized REE and primitive mantle-normalized trace-element patterns for the (a) Songshutang and (b) Wushitou ultramafic-mafic rocks in the SCB. Normalized values for chondrite and primitive mantle are from Sun & McDonough (1989); data for Ordovician appinites in Wugongshan (WGS) in the SCB are from Zhong *et al.* (2014); data for Silurian gabbro in Guangdong (GD) province are from Wang *et al.* (2013b); data for Silurian basalt in northern GD are from Yao *et al.* (2012); data for Silurian gabbro in central Fujian (FJ) province are from Zhang, Q. *et al.* (2015). Sampling locations of mafic rocks in the SCB are presented in Figure 1.

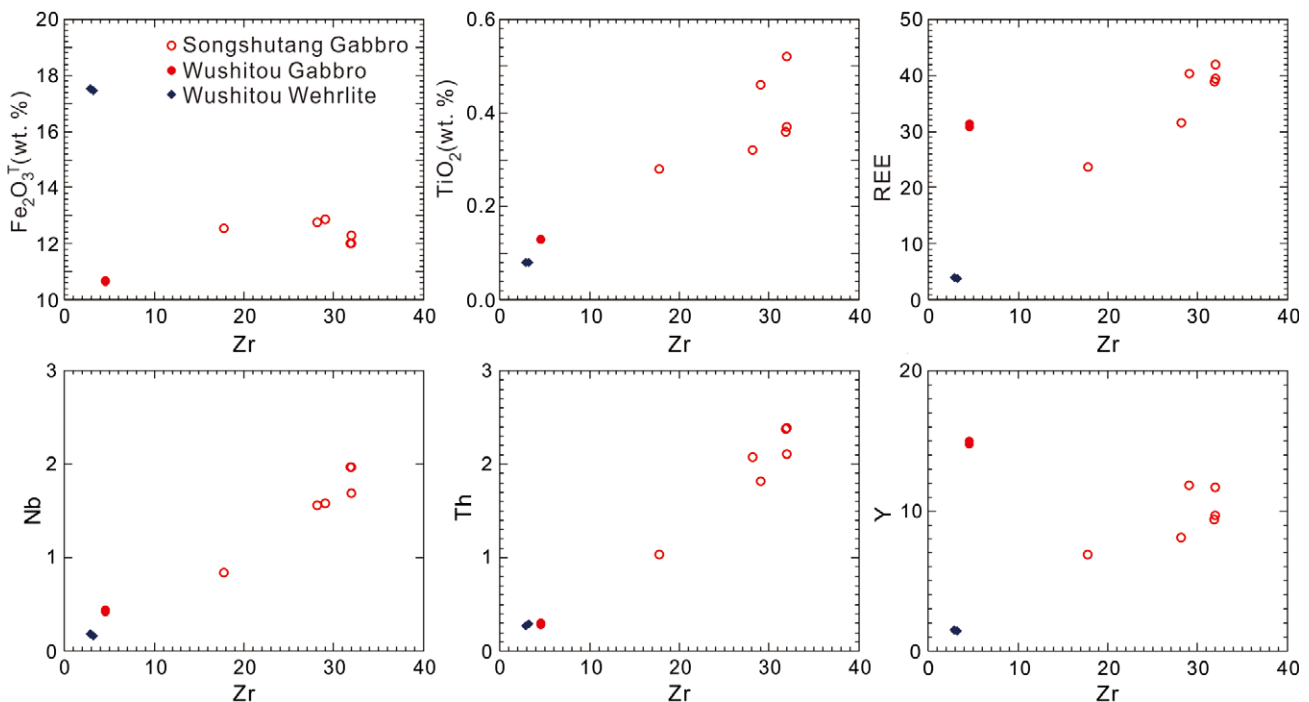


Fig. 7. (Colour online) Fe₂O₃^T, TiO₂, REEs, Nb, Th and Y versus Zr for the Songshutang and Wushitou ultramafic-mafic suites in the SCB.

¹⁷⁶Hf/¹⁷⁷Hf ratios from 0.282257 to 0.282437 and $\epsilon_{\text{Hf}}(t)$ values from -9.20 to -2.58 with corresponding Hf two-stage model ages ($T_{\text{DM}2}$) from 1991 to 1586 Ma. Nine analysis spots from sample G07-5 yielded ¹⁷⁶Hf/¹⁷⁷Hf ratios from 0.282203 to 0.282435 and $\epsilon_{\text{Hf}}(t)$ values from -10.84 to -4.21 and provided corresponding $T_{\text{DM}2}$ ages from 2099 to 1676 Ma. Eleven analysis spots from sample G10-1 gave ¹⁷⁶Hf/¹⁷⁷Hf ratios from 0.282274 to 0.282367 and yielded negative $\epsilon_{\text{Hf}}(t)$ values ranging from -8.67 to -5.19 with corresponding $T_{\text{DM}2}$ ages from 1947 to 1745 Ma.

5.c. Whole-rock major and trace elements

The whole-rock major- and trace-element compositions of the Songshutang and Wushitou ultramafic-mafic rocks are listed in online Supplementary Material Table S4 and Figures 6–9. Although we selected very fresh samples for the geochemical analyses, these ultramafic-mafic rocks have LOI concentrations ranging from 3.93–7.68 wt %, which display some plagioclase alteration. Two wehrlite samples from the Wushitou area have LOI concentrations of more than 10 % and will not be emphasized in the

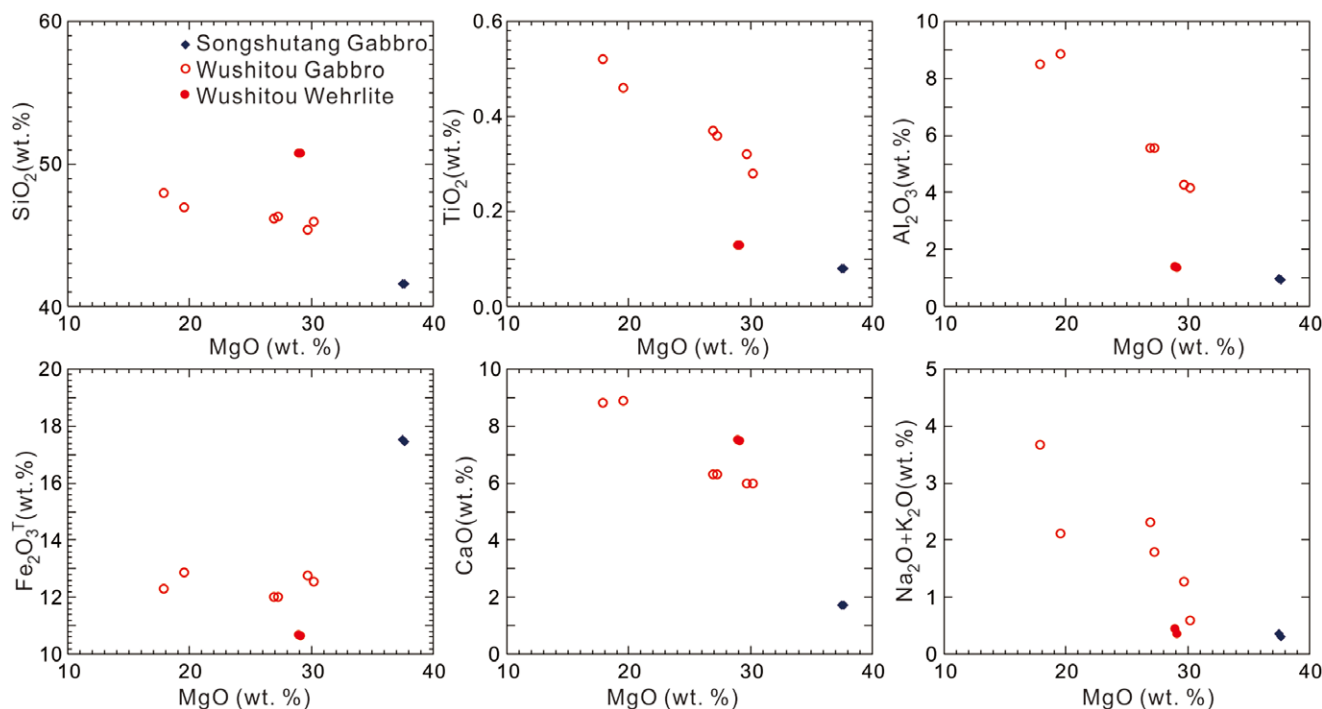


Fig. 8. (Colour online) MgO versus selected major and trace elements for the Songshutang and Wushitou ultramafic–mafic suites in the SCB.

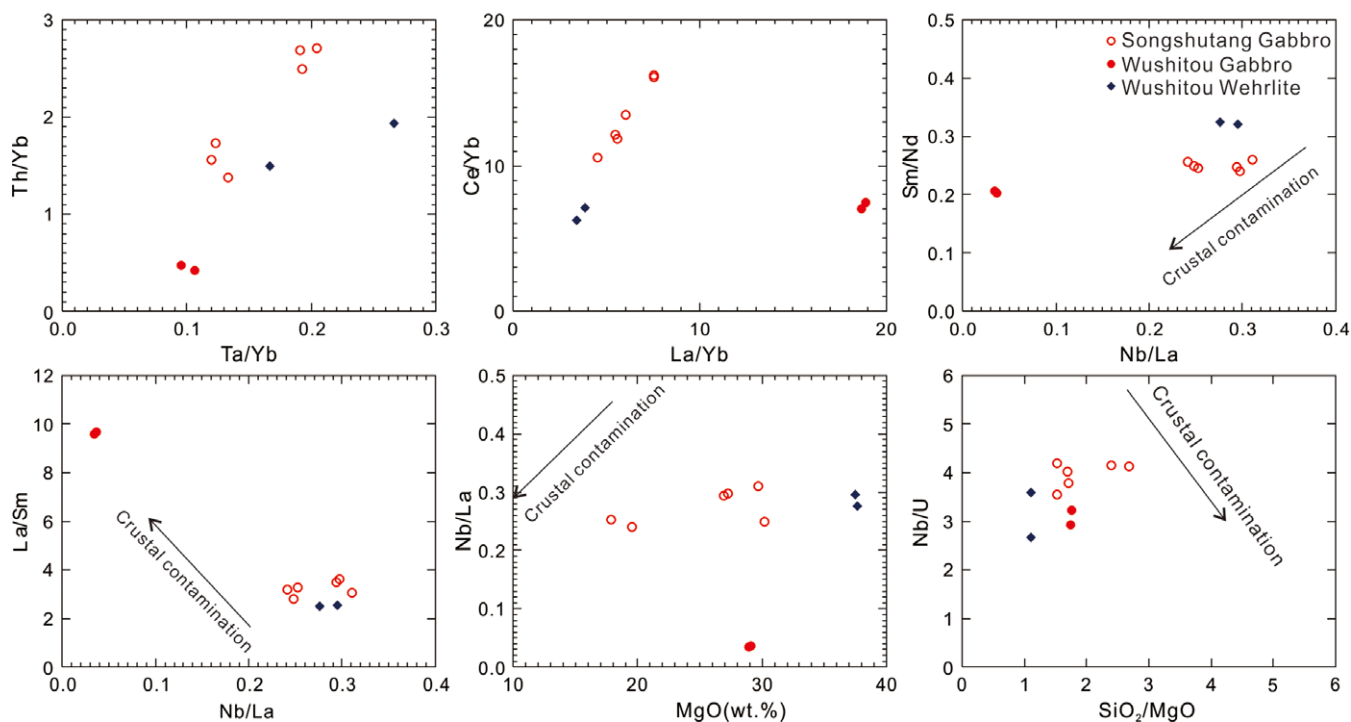


Fig. 9. (Colour online) (a) Th/Yb versus Ta/Yb, (b) Ce/Yb versus La/Yb, (c) Sm/Nd versus Nb/La, (d) La/Sm versus Nb/La, (e) Nb/La versus MgO and (f) Nb/U versus SiO₂/MgO diagrams for the Songshutang and Wushitou ultramafic–mafic suites in the SCB.

following discussions. Major-element values were recalculated on a volatile-free basis (online Supplementary Material Table S4). The Songshutang gabbroic samples have SiO₂ concentrations of 45.42–47.99 wt % (mean = 46.48 wt %), Al₂O₃ concentrations of 4.17–8.84 wt % (mean = 6.14 wt %), TiO₂ concentrations of 0.28–0.52 wt % (mean = 0.38 wt %), MgO concentrations of

17.87–30.19 wt % (mean = 25.26 wt %), CaO concentrations of 5.97–8.87 wt % (mean = 7.04 wt %), P₂O₅ concentrations of 0.08–0.16 wt % (mean = 0.13 wt %) and Mg nos of 74–83 (mean = 80). Compared to the Songshutang samples, the Wushitou samples have similar SiO₂ concentrations (mean = 46.16 wt %), higher MgO concentrations (mean = 33.30 wt %),

lower Al₂O₃ concentrations (mean = 1.17 wt %), lower TiO₂ concentrations (mean = 0.11 wt %), lower CaO concentrations (mean = 4.60 wt %), lower P₂O₅ concentrations (mean = 0.03 wt %) and higher Mg nos (81–85).

All Songshutang and Wushitou gabbroic rocks exhibit similar chondrite-normalized REE patterns, with total REE contents of 23.68–41.95 ppm, light REE/heavy REE (LREE/HREE) ratios of 3.88–5.31 and (La/Yb)_N ratios of 3.23–13.55 (Fig. 6a). Compared to the gabbroic rocks, the two wehrlite samples have lower total REE contents of 3.80–3.96 ppm, consistent with a large amount of olivine in the samples (Fig. 3c). Most analyses of samples from the Songshutang and Wushitou plutons have total LREE concentrations higher than those of the primitive mantle and normal mid-ocean ridge basalt (N-MORB) (Sun & McDonough, 1989). All samples from the Songshutang and Wushitou plutons exhibit negative Eu anomalies, with Eu/Eu* ratios of 0.69–0.88 and 0.45–0.67, respectively. On the primitive mantle-normalized spider diagram (Fig. 6b), all samples show a pattern with significant enrichments in Rb, Th, Ba and U and depletions in Nb, Ta, Zr, Hf and Ti, similar to those of the early Palaeozoic mafic rocks in the adjacent areas (Yao *et al.* 2012).

5.d. Whole-rock Sr–Nd isotopes

The whole-rock Sr–Nd isotope results are presented in online Supplementary Material Table S5. The Songshutang gabbroic samples have (⁸⁷Sr/⁸⁶Sr)_i ratios from 0.70435 to 0.70753, (¹⁴³Nd/¹⁴⁴Nd)_i values from 0.51161 to 0.51165, and ε_{Nd}(t) values from –9.12 to –8.27. One gabbro sample and one wehrlite sample from the Wushitou plutons were chosen for Sr–Nd isotope analysis owing to the extremely low Nd value (0.75 ppm) and the ¹⁴³Nd/¹⁴⁴Nd ratio of wehrlite sample G10-2, which is below the detection limit. The G10-2 sample has a (⁸⁷Sr/⁸⁶Sr)_i ratio of 0.71463. The G10-1 sample has a higher (⁸⁷Sr/⁸⁶Sr)_i value (0.71336), a higher (¹⁴³Nd/¹⁴⁴Nd)_i value (0.51179) and a higher ε_{Nd}(t) value (–5.49) than the Songshutang samples. The whole-rock Nd two-stage model ages (T_{DM2}) of the Songshutang and Wushitou mafic rocks were concentrated around ~1.9–1.6 Ga.

6. Discussion

6.a. Formation ages of the Songshutang and Wushitou ultramafic–mafic plutons

The Songshutang mafic pluton intruded into Cambrian Shuishi Formation siltstones, whereas the Wushitou ultramafic and mafic plutons intruded into Ediacaran migmatite and/or metamorphic rocks (Fig. 2). Thus, the Songshutang pluton was formed at least after the Cambrian, and the Wushitou intrusion formed later than the Ediacaran. Although no zircon age was obtained from the wehrlite in the Wushitou area and the contact relationship between the wehrlite and gabbro pluton in the Wushitou area remains unclear, the wehrlite and gabbro samples in the Wushitou area exhibit parallel chondrite-normalized REE patterns and LREE enrichment with slightly negative Eu anomalies, and on the primitive mantle-normalized spider diagram (Fig. 6b), all samples show a pattern with significant enrichments in Rb, Th, Ba and U and depletions in Nb, Ta, Zr, Hf and Ti. Therefore, the wehrlite in the Wushitou area most likely formed synchronously with the mafic intrusions in the Wushitou area. Furthermore, the zircon U–Pb ages of the Songshutang (G07-2, G07-3 and G07-5) and Wushitou (G10-1) gabbro and leucogabbro samples yielded consistent ²⁰⁶Pb–²³⁸U average ages of 437.8 ± 2.1 Ma, 437.3 ± 2.1 Ma,

437.8 ± 2.3 Ma and 437.8 ± 2.2 Ma, respectively, suggesting a Silurian (c. 437 Ma) formation age synchronous with the late-stage orogenic (440–415 Ma) felsic plutons (Li *et al.* 2010) and younger than the peak metamorphic ages of the Wuyi–Yunkai orogeny (460–440 Ma).

6.b. Evaluation of alteration, crystal fractionation and crustal contamination

The occurrence of secondary minerals, such as chlorite, serpentine, sericite and talc, and relatively high LOI percentages (online Supplementary Material Table S4) indicate that alteration could have been a possible factor modifying the geochemical compositions of the samples. The values of mobile elements, such as Cs, Rb, Ba, K and Sr, and large-ion lithophile elements (LILEs) could have been significantly changed and thus are likely unsuitable for discussing the petrogenesis of the Songshutang and Wushitou ultramafic–mafic plutons. Zr, as one of the most immobile elements during alteration, could be applied as an effective tracer of the mobility of other trace elements (Hastie *et al.* 2013). Thus, the extent of alteration could be expressed as correlations between selected trace elements and Zr. Major elements (Fe₂O₃^T, TiO₂), REEs and high-field-strength elements (HFSEs, such as Nb and Y) were correlated well with Zr (Fig. 7), suggesting that these elements were immobile during alteration and can be used to interpret the origin and evolution of the Songshutang and Wushitou ultramafic–mafic units.

In most oceanic basaltic rocks, the removal of olivine-rich assemblages could lead to the slight enrichment of silica in residual magmas, resulting in different MgO contents (e.g. Langmuir *et al.* 1992; Garcia *et al.* 1996). When the parental tholeiitic magmas cooled and evolved to a MgO content of ~9 %, the augite and plagioclase began crystallizing with olivine (Naumann & Geist, 1999). To further evaluate the effect of crystal fractionation, we examined MgO and selected major oxides in a binary diagram (Fig. 8). A positive correlation between MgO and Fe₂O₃^T, Ni and Co suggests that the samples could have experienced possible olivine crystal fractionation. A negative correlation between other major oxides (TiO₂, Al₂O₃ and CaO) and MgO suggests that the samples have no significant fractionation of plagioclase and Fe–Ti oxides (Fig. 8). Moreover, plagioclase fractionation in the primary melt will cause significant positive Eu anomalies; however, our samples have slightly negative Eu anomalies (Fig. 6), indicating that no plagioclase fractionation occurred in the primary melt.

Crystal fractionation combined with crustal contamination plays an important role in the evolution of magma, which may alter the isotopic and elemental compositions of magma (DePaolo, 1981; Zhao & Zhou, 2007). The enrichment of LILEs and depletion of HFSEs in our samples indicated that the Songshutang and Wushitou mafic rocks may have undergone crustal contamination. Th/Ta, Sm/Nd, Th/Yb, Ta/Yb, Ce/Yb, La/Sm, Nb/La and Nb/U ratios were used to evaluate the effect of crustal contamination (Campbell & Griffiths, 1993; Baker *et al.* 1997; Macdonald *et al.* 2001). As shown in Figure 9, the bivariate plots of Th/Yb versus Ta/Yb and Ce/Yb versus La/Yb exhibit positive correlations, which may have been caused by crustal contamination or derived from the lithospheric mantle. However, there is no significant correlation between Sm/Nd and Nb/La or between La/Sm and Nb/La, suggesting insignificant crustal contamination (Fig. 9).

6.c. Origin of the Wushitou and Songshutang ultramafic–mafic plutons

Basaltic primary melts are generally characterized by high Ni (> 400 ppm), Cr (> 1000 ppm) and Mg nos (73–81) (Sharma, 1997; Wilson, 1989). The Songshutang and Wushitou gabbros and wehrlite have high Ni (508–2942 ppm), Cr (1477–4520 ppm) and Mg nos (74–85), indicating a relatively primary melt origin. PRIMELT3 software was used to calculate the primary melt composition for the gabbro and wehrlite samples with the least alteration and crustal contamination. Two gabbro samples with low SiO₂ (< 50 wt %), low LOI (< 5 wt %), high Mg nos (74–85), high CaO (> 7 wt %), high Ni (> 500 ppm) and high Cr (> 1400 ppm) were chosen as initial materials to constrain the composition of the primary melt. $KD (Fe/Mg)^{oliv/liq}$ was chosen as 0.299–0.302, assuming that $Fe^{2+}/\Sigma Fe = 0.90$ in the melt (Herzberg & Asimow, 2015). The calculated primary basaltic melt comprises 46–50 % SiO₂, 22.6–28.9 % MgO, 9.6–11.4 % Fe₂O₃^T and 0.13–0.44 % TiO₂.

It is generally accepted that ultramafic–mafic rocks are typically derived from the lithospheric mantle or asthenospheric mantle (e.g. Sklyarov *et al.* 2003; Zhao & Zhou, 2007). The Nb/La ratio is a good index to distinguish lithospheric mantle and asthenospheric mantle contributions, as lithospheric mantle-derived melts are generally characterized by low Nb/La ratios, whereas asthenospheric mantle-derived melts have relatively high Nb/La ratios (Sun & McDonough, 1989; Cui *et al.* 2015). All Songshutang and Wushitou ultramafic–mafic rocks have nearly constant and relatively low Nb/La ratios (0.24–0.31), similar to typical lithospheric mantle-derived melts (~0.3; Cui *et al.* 2015). Depletions in Nb, Ta, Zr, Hf and Ti (Fig. 6) suggest that the magma source may have experienced melt/fluid interaction before partial melting. Moreover, the Songshutang and Wushitou samples have relatively low $\epsilon_{Nd}(t)$ values ranging from –9.12 to –5.49 and high initial ⁸⁷Sr/⁸⁶Sr ratios ($(^{87}Sr/^{86}Sr)_i = 0.70435$ to 0.71463) (online Supplementary Material Table S5), which are comparable to those of typical melt from the lithospheric mantle (Depaolo & Daley, 2000). In the diagram of $\epsilon_{Nd}(t)$ versus $(^{87}Sr/^{86}Sr)_i$, the Songshutang and Wushitou gabbros overlap with the potassic rocks in the Roccamonfina, Batu Tara and Roman regions, which originated from enriched lithospheric mantle related to subducted slab-derived melts (Nelson, 1992; Zhang, Q. *et al.* 2015; Fig. 10). Thus, the primary melts of the Songshutang–Wushitou samples were likely modified by subduction-derived components.

In contrast, the Songshutang and Wushitou ultramafic–mafic rocks have relatively low TiO₂ contents (0.07–0.49 wt %) and plot within the field of experimental refractory peridotite melts on the diagram of TiO₂ versus total Fe₂O₃ (Fig. 11a), also indicating a lithospheric mantle origin (Falloon *et al.* 1988). The relatively high Rb/Sr and low Ba/Rb in Figure 11b suggest a phlogopite-bearing source (Furman & Graham, 1999), consistent with our petrographic observations that the samples contain amphibole, indicating that the primary magma was hydrous (Zhang, Q. *et al.* 2015). Note also that the relatively low TiO₂ values, the enrichment in LILEs and LREEs, and the depletion of HFSEs in our samples are similar to those of subduction-derived arc-type magmatic rocks (e.g. Cox, 1980; Hole *et al.* 1984), which could be caused by ancient subduction, because the geological observations in South China reject the development of young and hot slab subduction during early–middle Palaeozoic time (Wang *et al.* 2013b). On the Th/Yb versus Nb/Yb diagram (Fig. 12), all samples plot entirely above the MORB–OIB array, indicating that the magma source may have been modified by subduction-derived fluids or melts

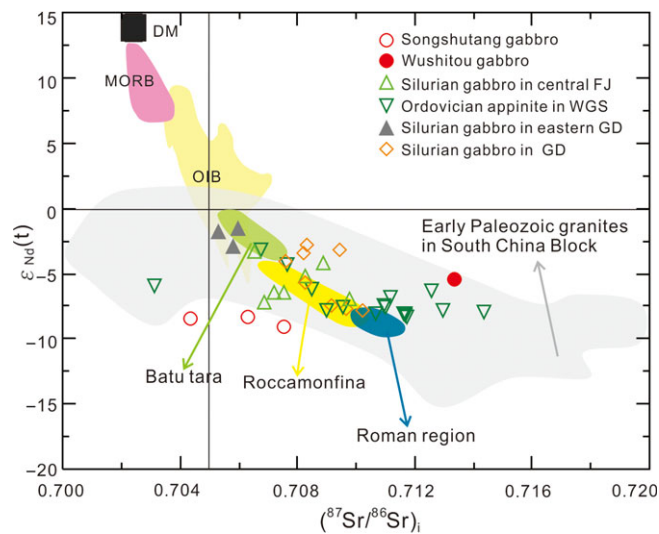


Fig. 10. (Colour online) Plots of whole-rock $\epsilon_{Nd}(t)$ versus initial $(^{87}Sr/^{86}Sr)_i$ for the Songshutang and Wushitou ultramafic–mafic suites in the SCB. Data for Ordovician appinites in Wugongshan (WGS) in the SCB from Zhong *et al.* (2014); data for Silurian gabbro in Guangdong (GD) province are from Wang *et al.* (2013b); data for Silurian gabbro in central Fujian (FJ) province are from Zhang, Q. *et al.* (2015); data for gabbro in eastern GD are from Xu *et al.* (2017); data for the Roccamonfina, Roman region and Batu Tara are from Nelson (1992); data for early Palaeozoic granites in the SCB are from Wang *et al.* (2013a and references therein).

(Pearce & Peate, 1995). Additionally, the Songshutang and Wushitou ultramafic–mafic rocks comprise relatively low Nb/La ratios (0.24–0.31 and 0.03–0.30, respectively) and Nb/Th ratios (0.75–0.86 and 0.55–1.49, respectively) but high Th/Ta ratio (10.34–14.36 and 4.13–8.22, respectively) and LREE/HREE ratios (3.88–5.31 and 2.79–5.04, respectively), consistent with those of subduction-derived melts (e.g. Kessel *et al.* 2005; Yao *et al.* 2012). Thus, the ancient subduction process possibly resulted in the interaction between subduction-derived fluids (or melts) and lithospheric mantle, further leading to lithospheric mantle enrichment in incompatible elements and hydrous phases.

The refractory nature of zircon enables this mineral, despite experiencing multistage tectonic–thermal events, to retain its initial Hf isotopic information, and thus zircon Hf isotopic compositions are generally used to track the origin and evolution of magma (e.g. Patchett *et al.* 1982; Scherer *et al.* 2000). The ¹⁷⁶Lu/¹⁷⁷Hf ratios of the Songshutang and Wushitou mafic rocks vary from 0.0009 to 0.0061 and from 0.001 to 0.003, respectively (online Supplementary Material Table S3), with extremely low Lu contents, suggesting that the ¹⁷⁶Hf resulting from the beta decay of ¹⁷⁶Lu is imperceptible. This corroborates that the ¹⁷⁶Lu/¹⁷⁷Hf ratios can reflect the initial values of the zircon (Hu *et al.* 2012). The Hf single-stage model ages (T_{DM1} , 1.5–1.1 Ga) and Hf two-stage model ages (T_{DM2} , 2.1–1.6 Ga, respectively) of the Songshutang and Wushitou samples are much older than their zircon U–Pb ages (c. 437 Ma), indicating that the protoliths of the samples may have originated from ancient lithospheric mantle. The whole-rock Nd two-stage model ages (T_{DM2} , 1.9–1.6 Ma) also confirm that the plutons were derived from ancient lithospheric mantle.

In addition, all the zircon Hf isotopic compositions of the Songshutang and Wushitou samples show negative $\epsilon_{Hf}(t)$ values (with $\epsilon_{Hf}(t)$ values of –10.84 to –2.58), and the plotted points on the $\epsilon_{Hf}(t)$ value versus crystallization age diagrams are primarily located below the chondritic uniform reservoir (CHUR) in a narrow domain near the evolutionary trends of c. 1.8 Ga crustal rocks

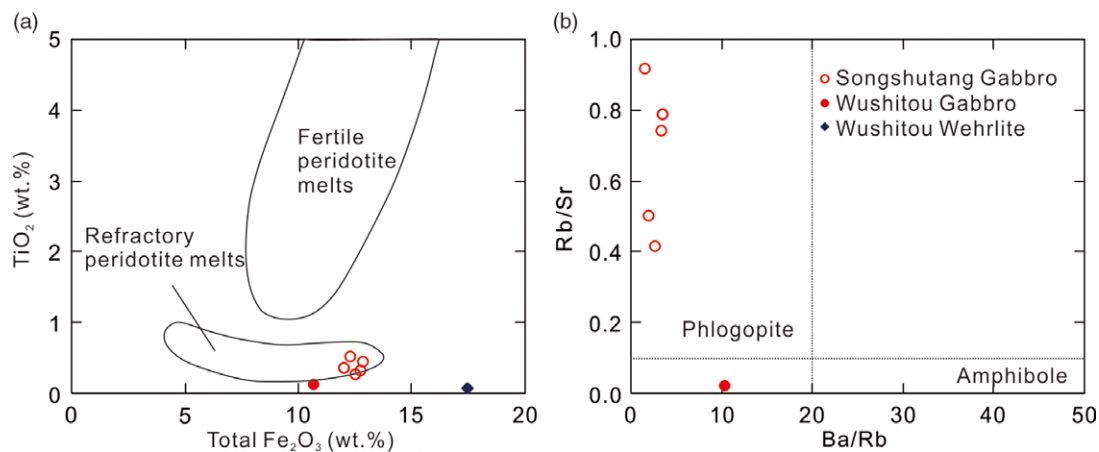


Fig. 11. (Colour online) Plots of (a) TiO_2 versus Fe_2O_3^T and (b) Rb/Sr versus Ba/Rb for the Songshutang and Wushitou ultramafic–mafic suites in the SCB. The fields of experimental peridotite melt in (a) are from Falloon *et al.* (1988) and Zhang, Q. *et al.* (2015) and the fields of phlogopite and amphibole in (b) are from Furman & Graham (1999).

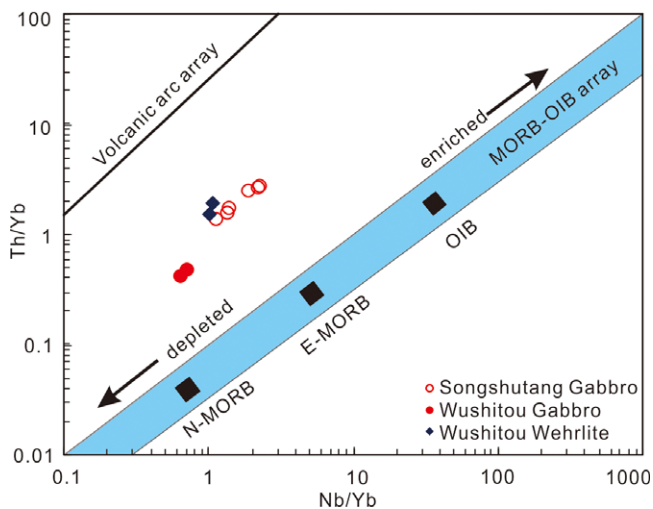


Fig. 12. (Colour online) Th/Yb versus Nb/Yb diagram (modified from Pearce & Peate, 1995). N – normal; E – enriched; MORB – mid-ocean ridge basalts; OIB – ocean-island basalts.

(Fig. 5). In addition, almost all Ordovician and Silurian mafic rocks in the SCB comprise low $\epsilon_{\text{Hf}}(t)$ values (< 0) (Fig. 13), and the Hf two-stage model ages ($T_{\text{DM}2}$) are mainly focused at ~ 2 – 1.1 Ga (Wang *et al.* 2013b; Zhong *et al.* 2014; Zhang, Q. *et al.* 2015; Xu *et al.* 2017 and this study). Most of the zircons (*c.* 480–420 Ma) from the early Palaeozoic mafic rocks in the SCB plot between the evolution lines of the average continental crust and chondrite (Fig. 13 and references therein). Moreover, the whole-rock Nd two-stage model ages ($T_{\text{DM}2}$) of the early Palaeozoic mafic rocks are concentrated at ~ 1.9 – 1.4 Ga (Yao *et al.* 2012; Wang *et al.* 2013b; Zhong *et al.* 2014; Zhang, Q. *et al.* 2015 and this study). These results suggest an ancient (Meso-Palaeoproterozoic) metasomatized lithospheric mantle origin for most of the early Palaeozoic mafic rocks in South China.

6.d. Timing, petrogenesis and tectonic implications for the Wuyi–Yunkai orogeny

The lack of an early Palaeozoic ophiolite suite and deep-sea marine sediments (turbidite sedimentary records) in the SCB

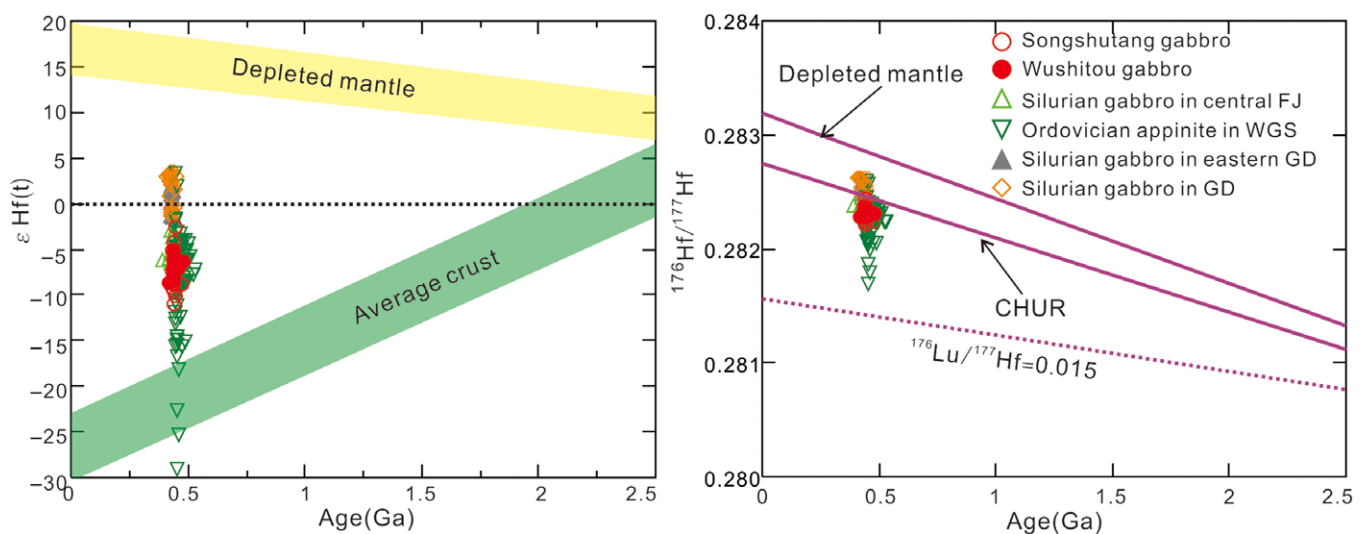


Fig. 13. (Colour online) Plots of $\epsilon_{\text{Hf}}(t)$ and $^{176}\text{Hf}/^{177}\text{Hf}$ versus U–Pb age for zircons from the Songshutang and Wushitou ultramafic–mafic suites in the SCB. Data for Ordovician appinites in Wugongshan (WGS) in the SCB are from Zhong *et al.* (2014); data for Silurian gabbro in Guangdong (GD) province are from Wang *et al.* (2013b); data for Silurian gabbro in central Fujian (FJ) province are from Zhang, Q. *et al.* (2015); data for gabbro in eastern GD are from Xu *et al.* (2017). CHUR – chondritic uniform reservoir. Sampling locations of mafic rocks in the SCB are presented in Figure 1.

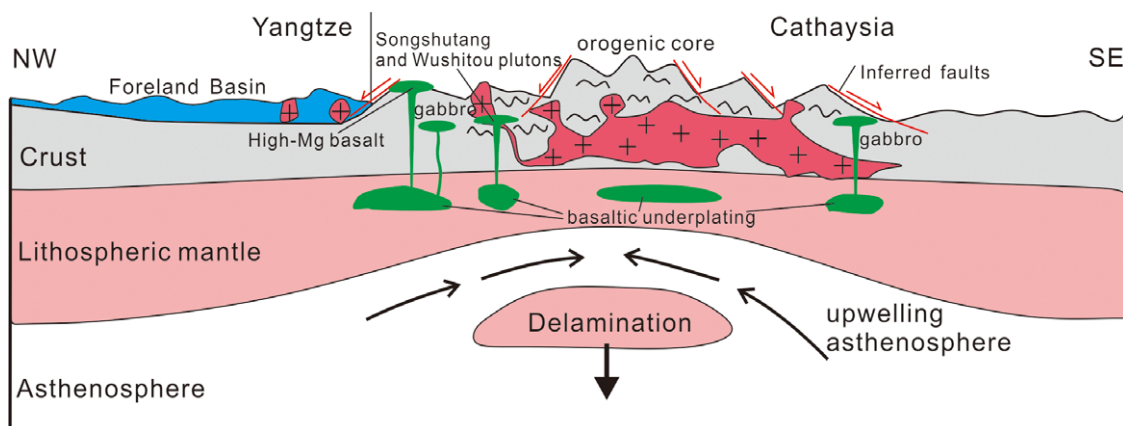


Fig. 14. (Colour online) Sketch showing the possible evolutionary model of the Wuyi–Yunkai orogen during the late-orogenic stage (442–420 Ma), modified from Charvet *et al.* (2010), Li *et al.* (2010) and Yao *et al.* (2012).

demonstrates that no subduction activity occurred during early Palaeozoic time in the SCB and that the orogen was an intraplate collision orogen caused by far-field tectonic stress (e.g. Faure *et al.* 2009; Li *et al.* 2010; Yao *et al.* 2012; Wang *et al.* 2013a; Xu *et al.* 2014). The mechanism of lithospheric mantle melting during the late orogeny was caused by late-orogenic collapse or lithospheric delamination in an intracontinental regime (Fig. 14; Yao *et al.* 2012; Wang *et al.* 2013b; Zhang, Q. *et al.* 2015). The estimated melting temperature for the early Palaeozoic mafic rocks in the SCB is ~ 1300 °C, similar to a MORB-like asthenospheric mantle (McKenzie & Bickle, 1988), supporting the hypothesis that the partially molten lithospheric mantle was heated by upwelling asthenosphere triggered by the sinking of the delaminated lithosphere (Yao *et al.* 2012; Zhang, Q. *et al.* 2015). Variation trends in the plots of MgO versus Cr, Ni, Co, SiO₂, TiO₂, CaO, Al₂O₃, CaO/Al₂O₃ and Fe₂O₃^T (Fig. 8) indicate that the early Palaeozoic ultramafic–mafic units in the SCB were derived from the same melts in different fractional crystallization stages. The high MgO values of the Songshutang and Wushitou ultramafic–mafic units were possibly the first-stage products of the metasomatized lithospheric mantle sources (Fig. 8) with slight mineral (olivine) fractional crystallization from the primary melt, and then they formed the Chayuanshan basalt and the gabbroic rocks in the Dakang, Guiyang and Yunkai belts in South China (Fig. 1) with olivine and clinopyroxene fractional crystallization. Further evolution of these melts was shown to have formed dacite rocks in the SCB (Yao *et al.* 2012).

In conclusion, lithospheric delamination is the most likely model for the post-extension of the Wuyi–Yunkai orogen, which also resulted in rapid exhumation (retrograde metamorphism), crustal uplift and extension (Zegers & van Keken, 2001). With post-extensional tectonism, the upwelling of asthenospheric mantle induced partial melting of ancient lithospheric mantle forming ultramafic–mafic rocks in the Jiangxi (Songshutang and Wushitung), Guangdong and Fujian areas, also generated numerous I-type and S-type granites (442–406 Ma) in the metamorphic core of the Cathaysia Block (Fig. 14; Yao *et al.* 2012; Wang *et al.* 2013b; Zhang, Q. *et al.* 2015; Yu, Y. *et al.* 2018; Xu *et al.* 2019).

7. Conclusions

- (1) Zircon U–Pb dating of the Songshutang and Wushitou gabbros and leucogabbros yielded ²⁰⁶Pb–²³⁸U ages of 437.8 ± 2.1 Ma,

437.3 ± 2.1 Ma, 437.8 ± 2.3 Ma and 437.8 ± 2.2 Ma, which are synchronous with the late-orogenic (440–415 Ma) granitic plutons and younger than the peak metamorphic ages of the Wuyi–Yunkai orogeny (460–440 Ma) in the SCB.

- (2) Geochemical, geochronological and isotopic data for the samples indicate that the magma sources of the Songshutang and Wushitou ultramafic–mafic rocks likely originated from the partial melting of ancient metasomatized lithospheric mantle in early Palaeozoic time.
- (3) Late-orogenic lithospheric delamination was likely the main mechanism leading to the partial melting of the lithospheric mantle through the upwelling of the asthenospheric mantle and caused ultramafic–mafic rocks to form along the Wuyi–Yunkai orogenic belt. The high MgO values of the Songshutang ultramafic–mafic plutons were possibly the first-stage products of lithospheric mantle sources with slight olivine fractional crystallization from the primary melt.

Acknowledgements. Our thanks to Kathryn Goodenough and the two anonymous reviewers for their insightful suggestions and comments that greatly improved the manuscript. This work was financially supported by the China Postdoctoral Science Foundation (No. 2020M672087), National Natural Science Foundation of China (41972108), the Laboratory for Marine Mineral Resources, Qingdao National Laboratory for Marine Science and Technology (MMRZZ201804), Taishan Scholar Talent Team Support Plan for Advanced and Unique Discipline Areas, Major Scientific and Technological Innovation Projects of Shandong Province (2017CXGC1602, 2017CXGC1603), SDUST Research Fund (2015TDJH101) and the China Scholarship Council (201606410022). We are grateful to Yongsheng Liu and Zhaochu Hu for LA-ICP-MS analyses.

Supplementary material. To view supplementary material for this article, please visit <https://doi.org/10.1017/S0016756820001272>

References

- Baker JA, Menzies MA, Thirlwall MF and Macpherson CG (1997) Petrogenesis of Quaternary intraplate volcanism, Sana'a, Yemen: implications for plume–lithosphere interaction and polybaric melt hybridization. *Journal of Petrology* **38**, 1359–90.
- Campbell IH and Griffiths RW (1993) The evolution of the mantle's chemical structure. *Lithos* **30**, 389–99.
- Carter A, Roques D, Bristow C and Kinny P (2001) Understanding Mesozoic accretion in Southeast Asia: significance of Triassic thermotectonism (Indosinian orogeny) in Vietnam. *Geology* **29**, 211–14.

- Cawood PA, Wang Y, Xu Y and Zhao G** (2013) Locating South China in Rodinia and Gondwana: a fragment of greater India lithosphere? *Geology* **41**, 903–6.
- Charvet J** (2013) The Neoproterozoic–Early Paleozoic tectonic evolution of the South China Block: an overview. *Journal of Asian Earth Sciences* **74**, 198–209.
- Charvet J, Shu L, Faure M, Choulet F, Wang B, Lu H and Le Breton N** (2010) Structural development of the Lower Paleozoic belt of South China: genesis of an intracontinental orogen. *Journal of Asian Earth Sciences* **39**, 309–30.
- Chen X, Tong L, Zhang C, Zhu Q and Li Y** (2015) Retrograde garnet amphibolite from eclogite of the Zhejiang Longyou area: new evidence of the Caledonian orogenic event in the Cathaysia block. *Chinese Science Bulletin* **60**, 1207–17.
- Cox KG** (1980) A model for flood basalt vulcanism. *Journal of Petrology* **21**, 629–50.
- Cui X, Jiang X, Wang J, Wang X, Zhuo J, Deng Q, Liao S, Wu H, Jiang Z and Wei Y** (2015) Mid-Neoproterozoic diabase dykes from Xide in the western Yangtze Block, South China: new evidence for continental rifting related to the breakup of Rodinia supercontinent. *Precambrian Research* **268**, 339–56.
- DePaolo DJ** (1981) Trace element and isotopic effects of combined wallrock assimilation and fractional crystallization. *Earth and Planetary Science Letters* **53**, 189–202.
- DePaolo DJ and Daley EE** (2000) Neodymium isotopes in basalts of the southwest basin and range and lithospheric thinning during continental extension. *Chemical Geology* **169**, 157–85.
- Falloon TJ, Green DH, Hatton C and Harris K** (1988) Anhydrous partial melting of a fertile and depleted peridotite from 2 to 30 kb and application to basalt petrogenesis. *Journal of Petrology* **29**, 1257–82.
- Faure M, Shu L, Wang B, Charvet J, Choulet F and Monié P** (2009) Intracontinental subduction: a possible mechanism for the Early Palaeozoic orogen of SE China. *Terra Nova* **21**, 360–8.
- Feng SJ, Zhao KD, Ling HF, Chen PR, Chen WF, Sun T, Jiang SY and Pu W** (2014) Geochronology, elemental and Nd–Hf isotopic geochemistry of Devonian A-type granites in central Jiangxi, South China: constraints on petrogenesis and post-collisional extension of the Wuyi–Yunkai orogeny. *Lithos* **206–207**, 1–18.
- Furman T and Graham D** (1999) Erosion of lithospheric mantle beneath the East African Rift system: geochemical evidence from the Kivu volcanic province. In *Composition, Deep Structure and Evolution of Continents* (eds RD van der Hilst and WF McDonough), pp. 237–62. Developments in Geotectonics vol. 24. Amsterdam: Elsevier.
- Garcia MO, Foss DJP, West HB and Mahoney JJ** (1996) Geochemical and isotopic evolution of Loihi Volcano, Hawaii. *Journal of Petrology* **37**, 1647–74.
- Hastie AR, Mitchell SF, Treloar PJ, Kerr AC, Neill I and Barfod DN** (2013) Geochemical components in a Cretaceous island arc: the Th/La–(Ce/Ce*) Nd diagram and implications for subduction initiation in the inter-American region. *Lithos* **162**, 57–69.
- He WH, Tang TT, Yue ML, Deng JF, Pan GT, Xing GF, Luo MS, Xu YD, Wei Y, Zhang ZY, Xiao YF and Zhang KX** (2014) Sedimentary and tectonic evolution of Nanhuan–Permian in South China. *Earth Science (Journal of China University of Geosciences)* **39**, 929–53 (in Chinese with English abstract).
- Herzberg C and Asimow PD** (2015) PRIMELT3 MEGA.XLSM software for primary magma calculation: peridotite primary magma MgO contents from the liquidus to the solidus. *Geochemistry, Geophysics, Geosystems* **16**, 563–78.
- Hole MJ, Saunders AD, Marriner GF and Tarney J** (1984) Subduction of pelagic sediments: implications for the origin of Ce-anomalous basalts from the Mariana Islands. *Journal of the Geological Society, London* **141**, 453–72.
- Hoskin PWO and Ireland TR** (2000) Rare earth element chemistry of zircon and its use as a provenance indicator. *Geology* **28**, 627–30.
- Hoskin PWO and Schaltegger U** (2003) The composition of zircon and igneous and metamorphic petrogenesis. *Reviews in Mineralogy and Geochemistry* **53**, 27–62.
- Hu L, Cawood PA, Du Y, Xu Y, Wang C, Wang Z, Ma Q and Xu X** (2017) Permo-Triassic detrital records of South China and implications for the Indosinian events in East Asia. *Palaeogeography, Palaeoclimatology, Palaeoecology* **485**, 84–100.
- Hu L, Du Y, Cawood PA, Xu Y, Yu W, Zhu Y and Yang J** (2014) Drivers for late Paleozoic to early Mesozoic orogenesis in South China: constraints from the sedimentary record. *Tectonophysics* **618**, 107–20.
- Hu Z, Gao S, Liu Y, Hu S, Chen H and Yuan H** (2008) Signal enhancement in laser ablation ICP-MS by addition of nitrogen in the central channel gas. *Journal of Analytical Atomic Spectrometry* **23**, 1093–101.
- Hu Z, Liu Y, Gao S, Liu W, Zhang W, Tong X, Lin L, Zong K, Li M and Chen H** (2012) Improved in situ Hf isotope ratio analysis of zircon using newly designed X skimmer cone and jet sample cone in combination with the addition of nitrogen by laser ablation multiple collector ICP-MS. *Journal of Analytical Atomic Spectrometry* **27**, 1391–9.
- Hu PY, Zhai QG, Ren GM, Wang J and Tang Y** (2018) Late Ordovician high-Mg adakitic andesite in the western South China block: evidence of oceanic subduction. *International Geology Review* **60**, 1140–54.
- Huang T** (1980) An outline of the tectonic characteristics of China. *Continental Tectonics* **36**, 184–97.
- Huang D and Wang X** (2019) Reviews of geochronology, geochemistry, and geodynamic processes of Ordovician–Devonian granitic rocks in southeast China. *Journal of Asian Earth Sciences* **184**, 104001. doi: [10.1016/j.jseaes.2019.104001](https://doi.org/10.1016/j.jseaes.2019.104001).
- Jia XH, Wang XD and Yang WQ** (2017) Petrogenesis and geodynamic implications of the early Paleozoic potassic and ultrapotassic rocks in the South China Block. *Journal of Asian Earth Sciences* **135**, 80–94.
- Kessel R, Schmidt MW, Ulmer P and Pettke T** (2005) Trace element signature of subduction-zone fluids, melts and supercritical liquids at 120–180 km depth. *Nature* **437**, 724.
- Kim SW, Oh CW, Williams IS, Rubatto D, Ryu IC, Rajesh V, Kim CB, Guo J and Zhai M** (2006) Phanerozoic high-pressure eclogite and intermediate-pressure granulite facies metamorphism in the Gyeonggi Massif, South Korea: implications for the eastward extension of the Dabie–Sulu continental collision zone. *Lithos* **92**, 357–77.
- Langmuir CH, Klein EM and Plank T** (1992) Petrological systematics of mid-ocean ridge basalts: constraints on melt generation beneath ocean ridges. In *Mantle Flow and Melt Generation at Mid-Ocean Ridges* (eds J Phipps Morgan, DK Blackman and JM Sinton), pp. 183–280. American Geophysical Union, Geophysical Monograph vol. 71. Washington, DC, USA.
- Li HB, Jia D, Wu L, Zhang Y, Yin HW, Wei GQ and Li BL** (2013) Detrital zircon provenance of the Lower Yangtze foreland basin deposits: constraints on the evolution of the early Palaeozoic Wuyi–Yunkai orogenic belt in South China. *Geological Magazine* **150**, 959–74.
- Li ZX and Li XH** (2007) Formation of the 1300-km-wide intracontinental orogen and postorogenic magmatic province in Mesozoic South China: a flat-slab subduction model. *Geology* **35**, 179–82.
- Li ZX, Li X, Wartho JA, Clark C, Li W, Zhang CL and Bao C** (2010) Magmatic and metamorphic events during the Early Paleozoic Wuyi–Yunkai orogeny, southeastern South China; new age constraints and pressure–temperature conditions. *Geological Society of America Bulletin* **122**, 772–93.
- Li X, Li Z, Zhou H, Liu Y and Kinny PD** (2002) U–Pb zircon geochronology, geochemistry and Nd isotopic study of Neoproterozoic bimodal volcanic rocks in the Kangdian Rift of South China: implications for the initial rifting of Rodinia. *Precambrian Research* **113**, 135–54.
- Li L, Lin S, Li J, He J and Ge Y** (2017) Zircon U–Pb ages and Hf isotope compositions of the Chencai migmatite, central Zhejiang Province, South China: constraints on the early Palaeozoic orogeny. *Geological Magazine* **155**, 1377–93.
- Lin SF, Xing GF, Davis DW, Yin CQ, Wu ML, Li LM, Jiang Y and Chen ZH** (2018) Appalachian-style multi-terrane Wilson cycle model for the assembly of South China. *Geology* **46**, 319–22.
- Liu S, Peng S, Kusky T, Polat A and Han Q** (2018) Origin and tectonic implications of an Early Paleozoic (460–440 Ma) subduction-accretion shear zone in the northwestern Yunkai Domain, South China. *Lithos* **322**, 104–28.
- Liu X, Wang Q, Ma L, Yang JH, Guo GN, Ou Q and Wang J** (2020) Early Paleozoic intracontinental granites in the Guangzhou region of South China: partial melting of a metasediment-dominated crustal source. *Lithos* **376–377**, 105763. doi: [10.1016/j.lithos.2020.105763](https://doi.org/10.1016/j.lithos.2020.105763).
- Ma Q, Zheng J, Griffin WL, Zhang M, Tang H, Su Y and Ping X** (2012) Triassic “adakitic” rocks in an extensional setting (North China): melts from the cratonic lower crust. *Lithos* **149**, 159–73.
- Macdonald R, Rogers NW, Fitton JG, Black S and Smith M** (2001) Plume–lithosphere interactions in the generation of the basalts of the Kenya Rift, East Africa. *Journal of Petrology* **42**, 877–900.

- McKenzie D and Bickle MJ (1988) The volume and composition of melt generated by extension of the lithosphere. *Journal of Petrology* **29**, 625–79.
- Naumann TR and Geist DJ (1999) Generation of alkalic basalt by crystal fractionation of tholeiitic magma. *Geology* **27**, 423–6.
- Nelson DR (1992) Isotopic characteristics of potassic rocks: evidence for the involvement of subducted sediments in magma genesis. *Lithos* **28**, 403–20.
- Ou Q, Lai JQ, Carvalho BB, Zi F, Kong H, Li B and Jiang ZQ (2018) Different response to middle-Palaeozoic magmatism during intracontinental orogenic processes: evidence from southeastern South China Block. *International Geology Review* **61**, 1504–21.
- Patchett PJ, Kouvo O, Hedge CE and Tatsumoto M (1982) Evolution of continental crust and mantle heterogeneity: evidence from Hf isotopes. *Contributions to Mineralogy and Petrology* **78**, 279–97.
- Pearce JA and Peate DW (1995) Tectonic implications of the composition of volcanic arc magmas. *Annual Review of Earth and Planetary Sciences* **23**, 251–85.
- Peng TP, Fan WM, Zhao GC, Peng BX, Xia XP and Mao YS (2015) Petrogenesis of the early Paleozoic strongly peraluminous granites in the Western South China Block and its tectonic implications. *Journal of Asian Earth Sciences* **98**, 399–420.
- Peng SB, Jin ZM, Fu JM, Liu YH, He LQ and Cai MH (2006) Geochemical characteristics of basic intrusive rocks in the Yunkai uplift, Guangdong–Guangxi, China, and their tectonic significance. *Geological Bulletin of China* **25**, 434–41 (in Chinese with English abstract).
- Peng SB, Liu SF, Lin MS, Wu CF and Han QS (2016) Early Paleozoic subduction in Cathaysia (II): new evidence from the Dashuang high magnesian–magnesian andesite. *Earth Science* **41**, 931–47 (in Chinese with English abstract).
- Qiu XF, Zhao XM, Yang HM, Lu SS, Jiang T and Wu NW (2018) Petrogenesis of the Early Palaeozoic granitoids from the Yunkai massif, South China block: implications for a tectonic transition from compression to extension during the Caledonian orogenic event. *Geological Magazine* **155**, 1776–92.
- Ren J (1991). On the geotectonics of southern China. *Acta Geologica Sinica (English Edition)* **4**, 111–30.
- Scherer EE, Cameron KL and Blichert TJ (2000) Lu–Hf garnet geochronology: closure temperature relative to the Sm–Nd system and the effects of trace mineral inclusions. *Geochimica et Cosmochimica Acta* **64**, 3413–32.
- Shan G, Rudnick RL, Hong LY, Xiao ML, Yong SL, Wen LX, Wen LL, John A, Xuan CW and Qing HW (2004) Recycling lower continental crust in the North China craton. *Nature* **432**, 892–7.
- Sharma M (1997) Siberian traps. In *Large Igneous Provinces: Continental, Oceanic and Planetary Flood Volcanism* (eds JJ Mahoney and MF Coffin), pp. 273–95. American Geophysical Union, Geophysical Monograph vol. 100. Washington, DC, USA.
- Shu L, Wang B, Cawood PA, Santosh M and Xu Z (2015) Early Paleozoic and Early Mesozoic intraplate tectonic and magmatic events in the Cathaysia Block, South China. *Tectonics* **34**, 1600–21.
- Sklyarov EV, Gladkochub D, Mazukabzov A, Menshagin YV, Watanabe T and Pisarevsky S (2003) Neoproterozoic mafic dike swarms of the Sharyzhalgai metamorphic massif, southern Siberian craton. *Precambrian Research* **122**, 359–76.
- Song MJ, Shu LS, Santosh M and Li JY (2015) Late Early Paleozoic and Early Mesozoic intracontinental orogeny in the South China Craton: geochronological and geochemical evidence. *Lithos* **232**, 360–74.
- Sun SS and McDonough WF (1989) Chemical and isotopic systematics of oceanic basalts: implications for mantle composition and processes. In *Magmatism in the Ocean Basins* (eds AD Saunders and MJ Norry), pp. 313–45. Geological Society of London, Special Publication no. 42.
- Wang Y, Fan W, Zhang G and Zhang Y (2013a) Phanerozoic tectonics of the South China Block: key observations and controversies. *Gondwana Research* **23**, 1273–305.
- Wang Y, Fan W, Zhao G, Ji S and Peng T (2007) Zircon U–Pb geochronology of gneissic rocks in the Yunkai massif and its implications on the Caledonian event in the South China Block. *Gondwana Research* **12**, 404–16.
- Wang J and Li ZX (2003) History of Neoproterozoic rift basins in South China: implications for Rodinia break-up. *Precambrian Research* **122**, 141–58.
- Wang Y, Li G, Wang Q, Santosh M and Chen J (2020) Early Paleozoic granitoids from South China: implications for understanding the Wuyi–Yunkai orogen. *International Geology Review* **62**, 243–61.
- Wang J, Shu L and Yu J (2017) From the Neoproterozoic mafic rock to the Silurian high-grade metamorphic rock: evidence from zircon U–Pb geochronological, bulk-rock geochemical and mineral EPMA studies of Longyou garnet amphibolite in SE China. *Journal of Asian Earth Sciences* **141**, 7–23.
- Wang Y, Zhang A, Fan W, Zhang Y and Zhang Y (2013b) Origin of paleo-subduction-modified mantle for Silurian gabbro in the Cathaysia Block: geochronological and geochemical evidence. *Lithos* **160–161**, 37–54.
- Wilson M (1989) *Igneous Petrogenesis*. London: Chapman and Hall.
- Wu Y and Zheng Y (2004) Genesis of zircon and its constraints on interpretation of U–Pb age. *Science Bulletin* **49**, 1554–69.
- Xia Y, Xu X, Zou H and Liu L (2014) Early Paleozoic crust–mantle interaction and lithosphere delamination in South China Block: evidence from geochronology, geochemistry, and Sr–Nd–Hf isotopes of granites. *Lithos* **184–187**, 416–35.
- Xie Y, Ma Y, Zhao G, Xie C, Han Y, Li J, Liu Q, Yao J, Zhang Y and Lu Y (2020) Origin of the Heping granodiorite pluton: implications for syn-convergent extension and asthenosphere upwelling accompanying the early Paleozoic orogeny in South China. *Gondwana Research* **85**, 149–68.
- Xu YJ, Cawood PA and Du YS (2016) Intraplate orogenesis in response to Gondwana assembly: Kwangsi Orogeny, South China. *American Journal of Science* **316**, 329–62.
- Xu Y, Cawood PA, Du Y, Huang H and Wang X (2014) Early Paleozoic orogenesis along Gondwana's northern margin constrained by provenance data from South China. *Tectonophysics* **636**, 40–51.
- Xu C, Wang Y, Zhang Y, Xu W and Gan C (2019) Geochronological and geochemical constraints of Chidong Silurian gabbroic pluton in Yunkai domain and its tectonic implications. *Earth Science* **44**, 1202–15 (in Chinese with English abstract).
- Xu W and Xu X (2017) An early Paleozoic monzonite–granite suite in the South China block: implications for the intracontinental felsic magmatism. *Mineralogy and Petrology* **111**, 709–28.
- Xu W, Xu X and Zeng G (2017) Crustal contamination versus an enriched mantle source for intracontinental mafic rocks: insights from early Paleozoic mafic rocks of the South China Block. *Lithos* **286–287**, 388–95.
- Yang J, Lyons TW, Zeng Z, Odigie K, Bates S and Hu L (2019a) Geochemical constraints on the origin of Neoproterozoic cap carbonate in the Helan Mountains, North China: implications for mid-late Ediacaran glaciation? *Precambrian Research* **331**, 105361. doi: 10.1016/j.precamres.2019.105361.
- Yang J, Zeng Z, Cai X, Li Z, Li T, Meng F and He W (2013) Carbon and oxygen isotopes analyses for the Sinian carbonates in the Helan Mountain, North China. *Science Bulletin* **58**, 3943–55.
- Yang J, Zhu Q, Zeng Z and Wan L (2019b) Zircon U–Pb ages and Hf isotope compositions of the Neoproterozoic magmatic rocks in the Helan mountains, North China. *Geological Magazine* **156**, 2104–12.
- Yao WH and Li ZX (2016) Tectonostratigraphic history of the Ediacaran–Silurian Nanhua foreland basin in South China. *Tectonophysics* **674**, 31–51.
- Yao WH and Li ZX (2019) Tectonostratigraphy and provenance analysis to define the edge and evolution of the eastern Wuyi–Yunkai orogen, South China. *Geological Magazine* **156**, 83–98.
- Yao WH, Li ZX, Li WX, Wang XC, Li XH and Yang JH (2012) Post-kinematic lithospheric delamination of the Wuyi–Yunkai orogen in South China: evidence from ca. 435 Ma high-Mg basalts. *Lithos* **154**, 115–29.
- Yu Y, Huang XL, Sun M and He PL (2018) Petrogenesis of granitoids and associated xenoliths in the early Paleozoic Baoux and Enping plutons, South China: implications for the evolution of the Wuyi–Yunkai intracontinental orogen. *Journal of Asian Earth Sciences* **156**, 59–74.
- Yu P, Zhang Y, Zhou Y, Weinberg RF, Zheng Y and Yang W (2019). Melt evolution of crustal anatexis recorded by the early Paleozoic Baiyunshan migmatite–granite suite in South China. *Lithos* **332–333**, 83–98.
- Yu P, Zheng Y, Zhou Y, Chen B, Niu J and Yang W (2018) Zircon U–Pb geochronology and geochemistry of the metabasite and gabbro: implications for the Neoproterozoic and Paleozoic tectonic settings of the Qinzhou bay–Hangzhou bay suture zone, South China. *Geological Journal* **53**, 2219–39.

- Zegers TE and van Keken PE** (2001) Middle Archean continent formation by crustal delamination. *Geology* **29**, 1083–6.
- Zeng W, Zhang L, Zhou H, Zhong Z, Xiang H, Liu R, Jin S, Lü X and Li C** (2008) Caledonian reworking of Paleoproterozoic basement in the Cathaysia Block: constraints from zircon U–Pb dating, Hf isotopes and trace elements. *Chinese Science Bulletin* **53**, 895–904.
- Zhang Q, Jiang YH, Wang GC, Liu Z, Ni CY and Qing L** (2015) Origin of Silurian gabbros and I-type granites in central Fujian, SE China: implications for the evolution of the early Paleozoic orogen of South China. *Lithos* **216**, 285–97.
- Zhang J, Liu W, Yakymchuk C, Sa R, Zeng Z, Ding R, Tang G, Liu H, Xu Q and Wang Y** (2019) Partial melting and crustal deformation during the Early Paleozoic Wuyi–Yunkai Orogeny: insights from zircon U–Pb geochronology and structural analysis of the Fuhuling Migmatites in the Yunkai Region, South China. *Minerals* **9**, 621.
- Zhang CL, Santosh M, Zhu QB, Chen XY and Huang WC** (2015) The Gondwana connection of South China: evidence from monazite and zircon geochronology in the Cathaysia Block. *Gondwana Research* **28**, 1137–51.
- Zhang XS, Xu XS, Xia Y and Liu L** (2017) Early Paleozoic intracontinental orogeny and post-orogenic extension in the South China Block: insights from volcanic rocks. *Journal of Asian Earth Sciences* **141**, 24–42.
- Zhang J, Ye T, Li S, Yuan G, Dai C, Zhang H and Ma Y** (2016) The provenance and tectonic setting of the Lower Devonian sandstone of the Danlin Formation in Southeast Yangtze Plate, with implications for the Wuyi–Yunkai orogeny in South China Block. *Sedimentary Geology* **346**, 25–34.
- Zhang CL, Zhu QB, Chen XY and Ye HM** (2016) Ordovician arc-related mafic intrusions in South China: implications for plate subduction along the southeastern margin of South China in the Early Paleozoic. *Journal of Geology* **124**, 743–67.
- Zhao G and Cawood PA** (1999) Tectonothermal evolution of the Mayuan Assemblage in the Cathaysia Block; implications for Neoproterozoic collision-related assembly of the South China Craton. *American Journal of Science* **299**, 309–39.
- Zhao G and Cawood PA** (2012) Precambrian geology of China. *Precambrian Research* **222**, 13–54.
- Zhao L, Cui X, Zhai M, Zhou X and Liu B** (2019) Emplacement and metamorphism of the mafic rocks from the Chencai Terrane within the Cathaysia Block: implications for the Paleozoic orogenesis of the South China Block. *Journal of Asian Earth Sciences* **173**, 11–28.
- Zhao JH and Zhou MF** (2007) Geochemistry of Neoproterozoic mafic intrusions in the Panzhihua district (Sichuan Province, SW China): implications for subduction-related metasomatism in the upper mantle. *Precambrian Research* **152**, 27–47.
- Zhong Y, Ma C, Liu L, Zhao J, Zheng J, Nong J and Zhang Z** (2014) Ordovician appinites in the Wugongshan Domain of the Cathaysia Block, South China: geochronological and geochemical evidence for intrusion into a local extensional zone within an intracontinental regime. *Lithos* **198**, 202–16.
- Zhong YF, Ma CQ, Zhang C, Wang SM, She ZB, Liu L and Xu HJ** (2013) Zircon U–Pb age, Hf isotopic compositions and geochemistry of the Silurian Fengdingshan I-type granite pluton and Taoyuan mafic–felsic complex at the southeastern margin of the Yangtze Block. *Journal of Asian Earth Sciences* **74**, 11–24.